University of Liège
Faculty of Applied Sciences
Academic year 2021-2022

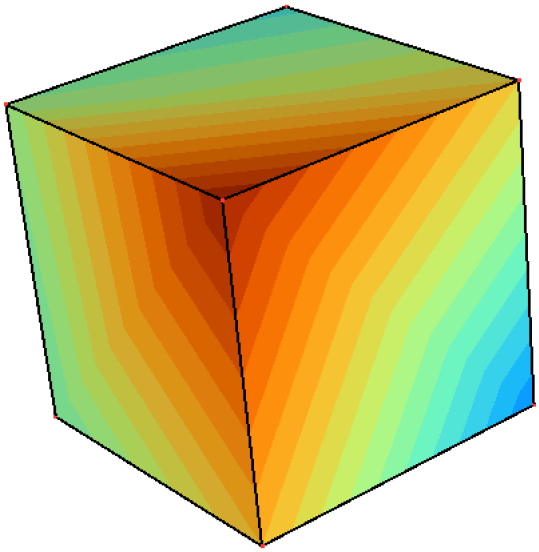

Cube in surface traction

Advanced Solid Mechanics

J-P. Ponthot

Nicolas Dujardin
Victor Mangeleer
Romain Gaspar
Ali Sezgin

Group 10

Contents

List of Figures

List of Tables

Introduction

This project has for purpose to introduce the plastic behavior of materials. Indeed, in solid mechanics, plasticity plays a major role in the explication of phenomenons such as irreversible deformation, fatigue and fracture. Therefore, it is important to take a grasp regarding this theory by performing numerical experiments on, for example, a cube under uniaxial surface traction. These experiments are done using the software *Metafor* which is an object-oriented finite element code for the simulation of solids submitted to large deformations.

The exploration of the plastic domain and its properties is done in four steps. First of all, the behavior of the cube is studied using linear hardening laws that can be purely isotropic, kinematic or a mix of them. Then, the same study is done but this time using non-linear hardening laws. These two parts will be done using an elasto-plastic model of the cube whereas for the following, this model is replaced by an elasto-viscoplastic one. In the third part, the idea is to study the effect of viscosity on the behavior of the deformation. Finally, the project is concluded by a study observing the influence of the different numerical parameters used to compute the simulations.

Furthermore, to make sure that the results of the simulations are physically plausible, they are compared directly to the one predicted by the theory. However, it is important to take into account that even if the simulations are in agreement with the theory, this does not imply that the model will satisfy reality. Indeed, a key element that is missing is to verify the correctness of the results by getting experimental results from laboratory. However, for the purpose of this introduction to plasticity, this project is limited to a comparison between theory and numerical simulations. In order to visualize the studied problem, Fig. 1 represents the cube under an uni-axial traction in the x-direction. In this case, the traction is supposedly uniform all over the surface.

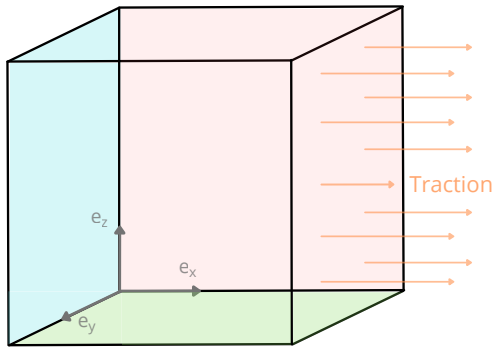

Figure 1: Representation of the cube undergoing an uni-axial surface traction. The colored surfaces represent the faces where the displacement is imposed to zero.

Data and numerical parameters

In this study, the considered system corresponds to a cube of side length equal to $S = 50$ [mm]. In addition to that, its physical properties as well as the numerical parameters used for the simulations are shown in the following Table.

$\bar{\varepsilon}^{vp}_{max}$ [%]	ρ [kg/m^3]	E [MPa]	ν [$-$]	σ^0_y [MPa]	h [MPa]	θ [$-$]	σ^∞_y [MPa]
0.4	7850	205000	0.3	200	30000	0.2	300

Table 1: Material properties and numerical parameters

Theoretical reminder and boundary conditions

Foremost, the study framework regarding the cube in traction, the different relevant variables, the assumptions and hardening models must be defined.

Model assumptions

The assumptions made for the analysis of the cube are listed as follows:

- Small deformations;
- The problem is considered as quasi-static and isothermal;
- There exists a yield function $f = f(\boldsymbol{\sigma}, \mathbf{q}) \leq 0$ determining the onset of plasticity where $\boldsymbol{\sigma}$ denote the state of stress and $\mathbf{q}$ denotes an internal variables that reflect the memory of the material. This yield function f is an indicator of the nature of loading process:
  - $f = f(\boldsymbol{\sigma}, \mathbf{q}) < 0 \quad \longrightarrow \quad$ elastic process;
  - $f = f(\boldsymbol{\sigma}, \mathbf{q}) = 0 \quad \longrightarrow \quad$ plastic process;
  - $f = f(\boldsymbol{\sigma}, \mathbf{q}) > 0 \quad \longrightarrow \quad$ forbidden process.
- An associated flow rule is considered such that the plastic flow potential is associated to the yield function f. Indeed, Melan and Prager assumed that the expression of the strain rate tensor can be expressed as:

$$D_{ij}^{p} = \dot{\tau} \frac{\partial g(\boldsymbol{\sigma}, \mathbf{q}, T)}{\partial \sigma_{ij}}, \tag{0.1}$$

  where $g(\boldsymbol{\sigma}, \mathbf{q}, T)$ is the flow potential and $\dot{\tau}$ is the plastic multiplier. This means that the plastic flow is in the direction of the normal to the hypersurface $g = 0$. Moreover, Drucker's postulate state that $D_{ij}^{p} = \dot{\gamma} \frac{\partial f}{\partial \sigma_{ij}}$ so that one can assume the plastic flow potential g is the same as the yield function f, this is called associated plasticity. In order to normalize the second order tensor $\frac{\partial g}{\partial \sigma_{ij}}$, one can introduce N_{ij} which corresponds to the flow direction and can be written as:

$$N_{ij} = \frac{\frac{\partial g}{\partial \sigma_{ij}}}{(\frac{\partial g}{\partial \boldsymbol{\sigma}} : \frac{\partial g}{\partial \boldsymbol{\sigma}})^{1/2}}, \tag{0.2}$$

  thus the Eq. 0.1 can be re-written as:

$$D_{ij}^{p} = \dot{\tau} \, (\frac{\partial g}{\partial \boldsymbol{\sigma}} : \frac{\partial g}{\partial \boldsymbol{\sigma}})^{\frac{1}{2}} N_{ij} = \lambda N_{ij}, \tag{0.3}$$

  where $\lambda = \dot{\tau} \, (\frac{\partial g}{\partial \sigma} : \frac{\partial g}{\partial \sigma})^{\frac{1}{2}}$ corresponds to the flow intensity. Similarly, one can write the evolution of the internal hardening variables $\mathbf{q}$ as:

$$\dot{\mathbf{q}}^{(k)} = \lambda \, r^{(k)}(\boldsymbol{\sigma}, \mathbf{q}). \tag{0.4}$$

Relevant variables

From now on, the focus is on describing the different relevant variables that will be used throughout the study. They are defined as follows:

- The yield stress σ_y corresponds to the maximum level of stress that can be reached before reaching plasticity. In the case of a virgin material, it is denoted as σ_y^0;
- The equivalent plastic strain $\bar{\varepsilon}^p(t)$ can be defined as:

$$\begin{aligned}\bar{\varepsilon}^p(t) &= \bar{\varepsilon}^p(t_0) + \int_{t_0}^{t_1} \sqrt{\frac{2}{3} D_{ij}^{vp} D_{ij}^{vp}}\, dt, \\ &= \bar{\varepsilon}^p(t_0) + \int_{t_0}^{t_1} \sqrt{\frac{2}{3} \lambda N_{ij} \lambda N_{ij}}\, dt, \\ &= \bar{\varepsilon}^p(t_0) + \int_{t_0}^{t_1} \sqrt{\frac{2}{3}}\lambda. \end{aligned} \tag{0.5}$$

  where, $\bar{\varepsilon}^p(t_0)$ is the equivalent plastic strain at time, equal to zero for the initial time and D_{ij}^{vp} is the plastic strain rate. From Eq. 0.5, it can be deduced that the equivalent plastic strain is a quantity that never decreases and corresponds to a measure of the plastic deformation in the material. The effective plastic strain rate can also be deduced from the former equation:

$$\dot{\bar{\varepsilon}}^p = \sqrt{\frac{2}{3}}\lambda \geq 0. \tag{0.6}$$

- The equivalent stress $\bar{\sigma}(t)$ corresponds to a measure of the state of stress in the materials and takes into account the deformation done to the yield surface. By denoting s_{ij} as the deviatoric tensor, the expression of $\bar{\sigma}(t)$ is thus given by:

$$\bar{\sigma}(t) = \sqrt{3J_2(s_{ij})}(t) = \sqrt{\frac{3}{2} s_{ij} s_{ij}}. \tag{0.7}$$

- The equivalent backstress $\bar{\alpha}(t)$ measures the translation of the center of the yield surface, its expression is:

$$\bar{\alpha}(t) = \sqrt{\frac{3}{2} \alpha_{ij} \alpha_{ij}}. \tag{0.8}$$

- The Von Mises' equivalent stress $\bar{\sigma}^{VM}(t)$ is similar to $\bar{\sigma}(t)$ but the difference is that it takes the position of the center of the yield surface into account, its expression is given by:

$$\bar{\sigma}^{\text{VM}}(t) = \sqrt{\frac{3}{2} \left(s_{ij} - \alpha_{ij}\right) \left(s_{ij} - \alpha_{ij}\right)}, \tag{0.9}$$

  with the deviatoric tensor $s_{ij} = \sigma_{ij} - p\delta_{ij}$ and $p = \sigma_{ii}/3$.

The hardening laws

Finally, the different hardening laws used in order to study the behaviour of the cube are the following:

- **Perfectly plastic model**

  A perfectly plastic material has no hardening at all such that the hardening parameter h is equal to zero. In this case, the yield criterion f can be written as:

  $$f = \sqrt{3J_2} - \sigma_y^0 = \bar{\sigma} - \sigma_y^0 \leq 0. \tag{0.10}$$

  In this case, as there is no hardening, the current yield stress is always equal to the initial yield stress of the virgin material:

  $$\sigma_{\mathrm{y}} = \sigma_{\mathrm{y}}^0. \tag{0.11}$$

  Geometrically, this means that the yield surface has a constant size and shape and its center does not translate in the stress space.

- **Isotropic linear hardening:**

  In a simple perfectly plastic model, the yield surface is fixed and rigid. From a physical point of views, this implies that the yield stress is not subjected to hardening. In order to represent the real behaviour of metals, some hardening laws must be introduced to represent plasticity and the deformation of the yield surface. The first considered law is the linear isotropic hardening, in this case the yield function is defined as:

  $$f = \bar{\sigma} - \sigma_y(\varepsilon^p) \leq 0. \tag{0.12}$$

  The subsequent yield stress will influence the radius of the yield surface and depends on the effective plastic strain,

  $$\sigma_{\mathrm{y}} = \sigma_{\mathrm{y}}^0 + h_i \bar{\varepsilon}^{vp}, \tag{0.13}$$

  where h_i is the linear isotropic hardening parameter whose expression is given by

  $$h_i = \frac{E E_T}{E - E_T} \; = \; C^{ste}, \tag{0.14}$$

  with E the young modulus and E_T the tangent modulus. As referred in the name of the hardening law, the expansion of the yield surface is uniform in all directions and the center of this yield surface does not translate, meaning that the back-stress tensor is $\alpha = 0$. The subsequent yield stress represents the modification of the size of the yield surface, therefore, the size vary with the equivalent plastic strain.

- **Kinematic linear hardening**

  By contrast to the isotropic linear hardening, the kinematic linear hardening model states that the size of the yield does not change but translates in the stress space during plastic deformation. Conversely to the previous hardening law, this model is able to represents the Bauschinger effect.

The yield function can be written as :

$$f(\sigma, \alpha, \sigma_y^0) = \sqrt{\frac{3}{2}(s_{ij} - \alpha_{ij})(s_{ij} - \alpha_{ij})} - \sigma_y^0 = \bar{\sigma}^{VM} - \sigma_y^0. \tag{0.15}$$

It is thus clear that the kinematic hardening models requires an evolution rule for the back-stress, which denotes the position of the center of the yield surface. The hardening law used to describe the kinematic hardening is presented by Drucker-Prager where the subsequent yield stress and the back-stress are defined as:

$$\sigma_{\mathrm{y}} = \sigma_{\mathrm{y}}^0 \quad \text{and} \quad \dot{\alpha}_{ij} = \frac{2}{3} h_k D_{ij}^{vp}. \tag{0.16}$$

with h_k the kinematic hardening parameter. The subsequent yield stress represents the modification of the size of the yield surface, therefore the size is constant and characterized by the virgin yield stress σ_y^0. The movement of the center of the yield surface is described by the back-stress tensor α_{ij}.

- **Mixed linear hardening**

  The last hardening model to consider is the mixed linear hardening, which combines the two previous hardening laws. The yield function is therefore :

$$f = \bar{\sigma}^{VM} - \sigma_y(\bar{\varepsilon}^p). \tag{0.17}$$

  The subsequent yield stress and the evolution of the back-stress, are defined exactly as in the Eq. 0.16. In this last model, the hardening coefficient h is subdivided between the isotropic or kinematic hardening using a weighting parameters θ, so $h_i = \theta h$ and $h_k = (1 - \theta)h$.

Plane stress

For the first state of stress, the force is applied on one face in the x direction as represented in Fig. 1. Moreover, there is no boundary condition preventing the deformation in one of the principal directions. Therefore, the problem corresponds to a uni-axial loading with $\sigma_x(t)$, the applied stress. The stress and strain tensor can be written as:

$$\boldsymbol{\sigma}(t) = \begin{pmatrix} \sigma_x(t) & 0 & 0 \\ 0 & 0 & 0 \\ 0 & 0 & 0 \end{pmatrix} \quad \text{and} \quad \boldsymbol{\varepsilon}(t) = \begin{pmatrix} \varepsilon_x(t) & 0 & 0 \\ 0 & \varepsilon_y(t) & 0 \\ 0 & 0 & \varepsilon_z(t) \end{pmatrix}. \tag{0.18}$$

The stress deviatoric tensor **s** can be computed as follows:

$$\mathbf{s} = \mathrm{dev}(\boldsymbol{\sigma}) = \boldsymbol{\sigma} - \frac{1}{3}\mathrm{tr}(\boldsymbol{\sigma}) \quad \Leftrightarrow \quad \boldsymbol{s}(t) = \begin{pmatrix} \frac{2}{3}\sigma_x(t) & 0 & 0 \\ 0 & -\frac{1}{3}\sigma_x(t) & 0 \\ 0 & 0 & -\frac{1}{3}\sigma_x(t) \end{pmatrix}. \tag{0.19}$$

Therefore, the second invariant of the deviatoric tensor, J_2 can be computed as:

$$J_2 = \frac{1}{2} s_{ij} s_{ij} = \frac{1}{3} \sigma_x^2(t). \tag{0.20}$$

It can be noticed that the general definition of $\bar{\sigma}(t)$ represented in Eq. 0.7 can be re-written as:

$$\bar{\sigma}(t) = \sqrt{3J_2} = |\sigma_x(t)|. \tag{0.21}$$

Finally, the general expression of the backstress tensor $\boldsymbol{\alpha}$ in plane stress state can be defined. Indeed, as the loading is applied in the x-direction, the tensor is diagonal and has the following form:

$$\boldsymbol{\alpha} = \begin{pmatrix} \alpha_x & 0 & 0 \\ 0 & \alpha_y & 0 \\ 0 & 0 & \alpha_z \end{pmatrix}. \tag{0.22}$$

Plane strain

In order to reach a plane strain state, the system has to verify the following relation:

$$\varepsilon_y = \frac{\partial u_y}{\partial x_y} = 0. \tag{0.23}$$

In this configuration, the deformation in the y-direction is blocked. The cube is therefore free to move only in the x and z-directions. That leads to a change in the stress and strain tensors since blocking the y-direction induces a stress in this same direction. The different tensors are now defined as follows:

$$\boldsymbol{\sigma}(t) = \begin{pmatrix} \sigma_x(t) & 0 & 0 \\ 0 & \sigma_y(t) & 0 \\ 0 & 0 & 0 \end{pmatrix} \quad \text{and} \quad \boldsymbol{\varepsilon}(t) = \begin{pmatrix} \varepsilon_x(t) & 0 & 0 \\ 0 & 0 & 0 \\ 0 & 0 & \varepsilon_z(t) \end{pmatrix}. \tag{0.24}$$

As before, the stress deviatoric tensor can be computed:

$$\boldsymbol{s}(t) = \begin{pmatrix} \frac{2}{3}\sigma_x(t) - \frac{1}{3}\sigma_z(t) & 0 & 0 \\ 0 & -\frac{1}{3}\sigma_x(t) + \frac{2}{3}\sigma_z(t) & 0 \\ 0 & 0 & -\frac{1}{3}\sigma_x(t) - \frac{1}{3}\sigma_z(t) \end{pmatrix}. \tag{0.25}$$

Part 1 - Study of elasto-plastic behavior with linear hardening

1.1 Analysis of the different plastic models

First of all, it is necessary to determine the maximum surface traction $t_{\max}$ characterizing the loading cycles. Such a surface traction allows to reach the maximum permanent plastic deformation $\bar{\varepsilon}^p_{\max}$ imposed by the geometry for an isotropic model. To do so, one needs to use $\bar{\varepsilon}^p = \bar{\varepsilon}^p_{max}$ to express the subsequent yield stress as:

$$t_{max} = \sigma^0_{\mathrm{y}} + h\, \bar{\varepsilon}^p_{max}, \tag{1.26}$$

where h and $\bar{\varepsilon}^p_{\max}$ are given in Table 1, which leads to $t_{\max} = 320$ [MPa]. Besides the surface traction, the cycles are characterized by their duration T and the number of repetitions N. Given the fact that there is no viscous process in this first part, the considered models are time insensitive and the period of a cycle is arbitrarily fixed at 5 [s]. The different types of plastic models can thus be studied by analyzing the results obtained from a simulation composed of 3 cycles.

1.1.1 Isotropic linear hardening

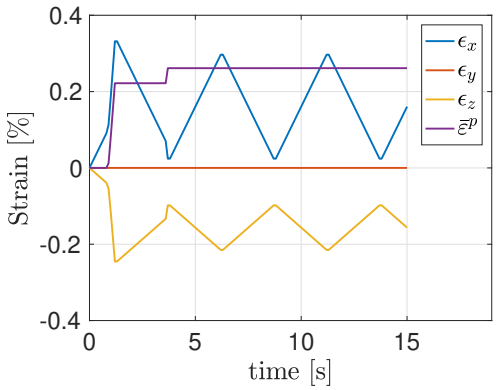

(a) Strain in plane strain state

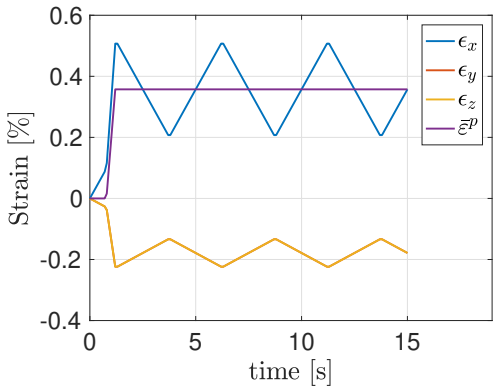

(b) Strain in plane stress state

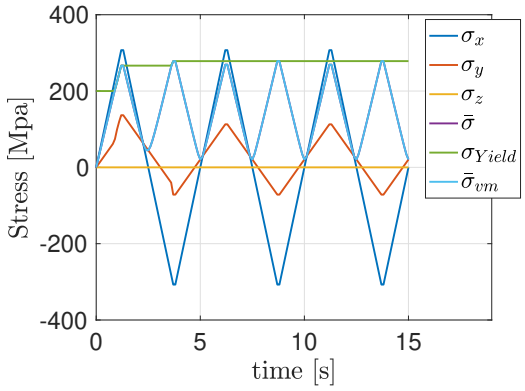

(c) Stress in plane strain state

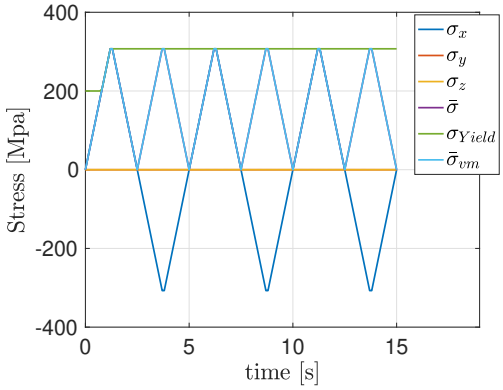

(d) Stress in plane stress state

Figure 2: Evolution of the strain and stress in the case of an isotropic linear hardening model with 3 cycles of 5 seconds. The results are represented either in plane strain or plane stress.

1.1.2 Kinematic linear hardening

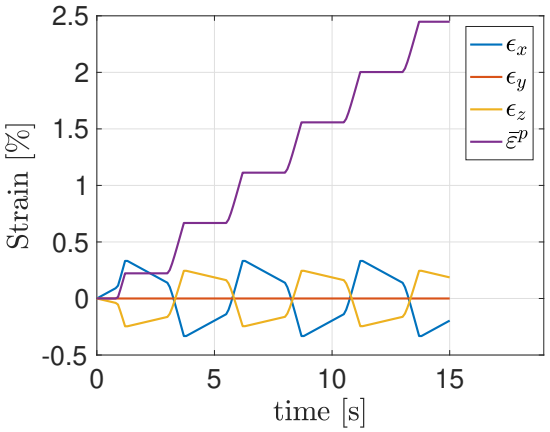

(a) Strain in plane strain state

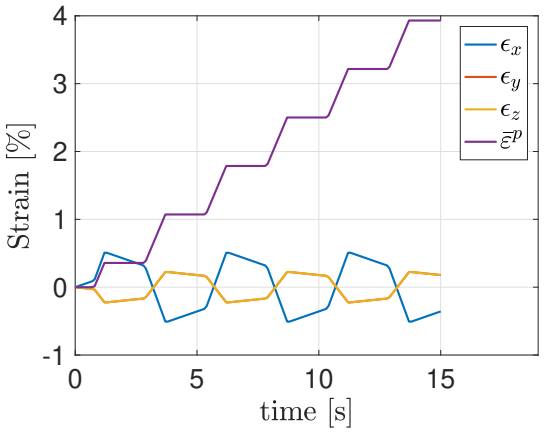

(b) Strain in plane stress state

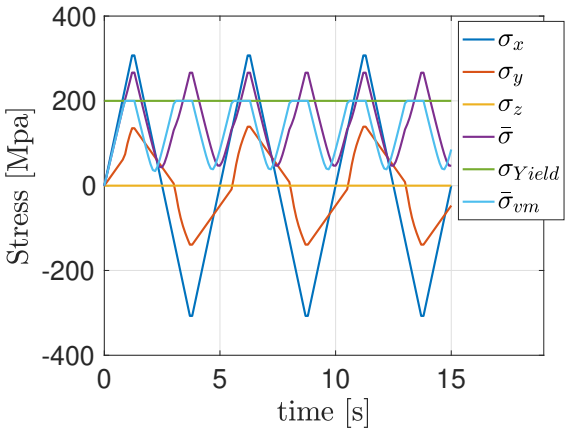

(c) Stress in plane strain state

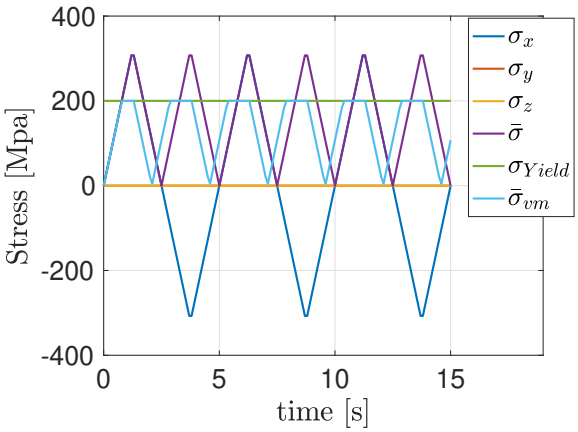

(d) Stress in plane stress state

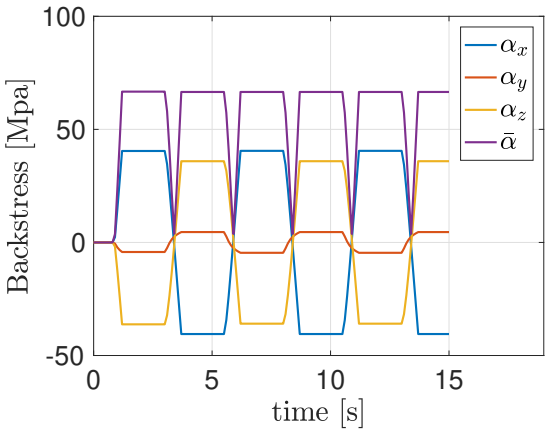

(e) Backstress in plane strain state

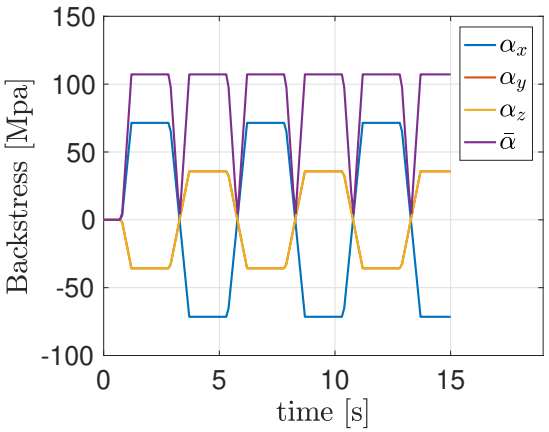

(f) Backstress in plane stress state

Figure 3: Evolution of the strain, stress and backstress in the case of a kinematic linear hardening model with 3 cycles of 5 seconds. The results are represented either in plane strain or plane stress.

1.1.3 Mixed linear hardening

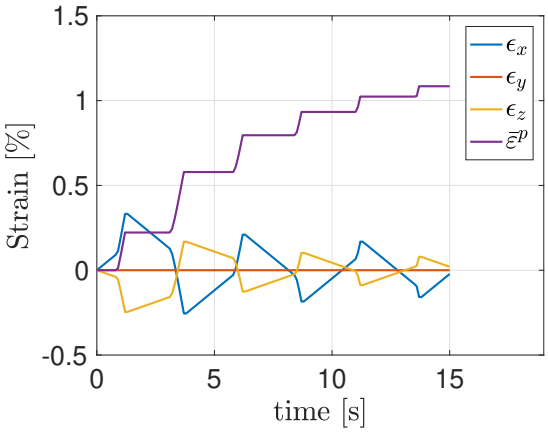

(a) Strain in plane strain state

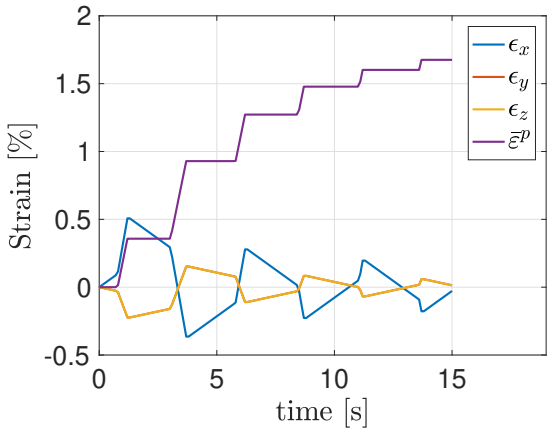

(b) Strain in plane stress state

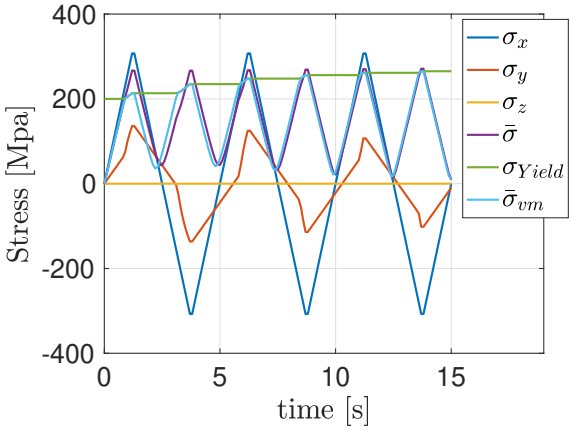

(c) Stress in plane strain state

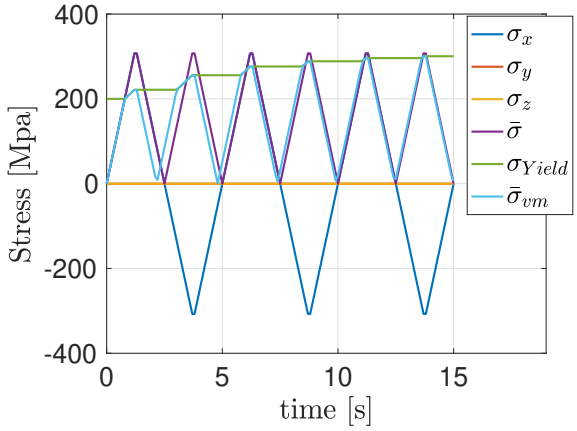

(d) Stress in plane stress state

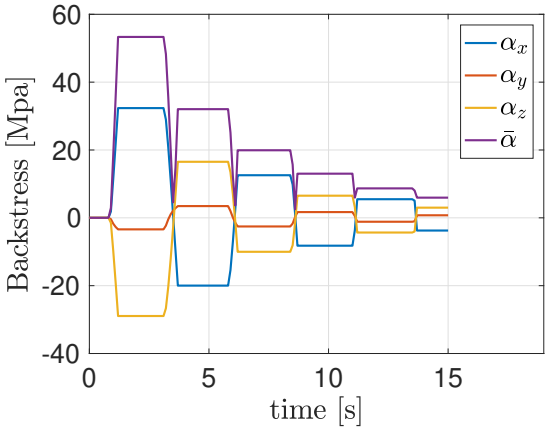

(e) Backstress in plane strain state

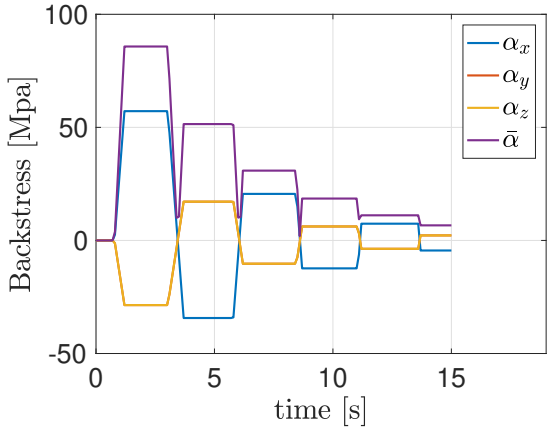

(f) Backstress in plane stress state

Figure 4: Evolution of the strain, stress and backstress in the case of a mixed linear hardening model with 3 cycles of 5 seconds. The results are represented either in plane strain or plane stress.

1.1.4 Perfectly plastic

In the case of the perfectly plastic model, the simulation leads to an abort. It can be explained by the fact that, once the plasticity reached, the deformations in the loading direction become so high that the software is not able to represent the model. From a physical point of view, it can be interpreted as the fracture of the cube.

1.1.5 Analysis

All the results are summarized in the following Table in order to easily compare all the models in plane strain state and in plane stress state.

	Isotropic		**Kinematic**		**Mixed**	
Plane state	Strain	Stress	Strain	Stress	Strain	Stress
$\bar{\varepsilon}^p(t_f)$ [%]	0.26	0.36	2.5	3.9	1.1	1.7
$\sigma^{yield}(t_f)$ [MPa]	278.4	307.2	200	200	265.1	300.5
First plateau value of $\bar{\alpha}(t)$ [MPa]	/	/	66.7	107.2	53.3	85.8
Last plateau value of $\bar{\alpha}(t)$ [MPa]	/	/	66.7	107.2	5.9	6.7

Table 2: Value of the variables for the three linear models in plane stress and strain states.

First, it can be noticed that the final plastic strain is in all cases larger in plane stress state than in plane strain state. This observation seems logical given that the displacement along the y-direction is blocked due to the boundary conditions imposed to ensure the equality $\varepsilon_y = 0$. It implies a non-zero stress component σ_y while the plane stress state is reduced to a uni-axial stress in the x-direction. In both states, the component σ_z is zero.

Afterwards, it can be easily noticed that the yield stress increases with the equivalent plastic strain in the isotropic and mixed case while it remains constant in the kinematic model. Its final value is one more time larger in the plane stress state such that the boundary conditions added in plane strain allow to reduce the plastic deformation.

Then, regarding the backstress, it only varies during the hardening process and stays on a plateau over the elastic range. The value of the plateau characterizes the translation of the yield surface over the hardening process. On one hand, the kinematic hardening presents several equal plateaus through the loading time, this value is greater in the plane stress case and the hardening effect is thus stronger than in the plane strain case. On the other hand, the plateau value decreases over the time in the mixed model, consequently the backstress effect decreases over time and the center of the surface tends to fix itself.

Finally, in all cases, the Von Mises criterion is well verified. Indeed, the Von Mises equivalent stress $\overline{\sigma}^{VM}$ is always lower or equal to the yield stress. It is good to remember that this variable is the relative stress state defined with respect to the center of the yield surface while the equivalent stress $\overline{\sigma}$ is the state regarding the origin. It is thus possible to get an equivalent stress $\overline{\sigma}$ larger than the yield stress σ^{yield} since the latter is the relative limit with respect to the center of the yield surface.

1.2 Geometric interpretation of the yield surface

To visualize the hardening process and better understand the previous observations, it is suitable to represent the evolution of the yield surface in Haigh Westergaard's space. Given that in all cases, the stress components $\sigma_z = 0$, the representation can be restricted to the plane (σ_x , σ_y). In this case, the Von Mises yield criterion writes:

$$\frac{3}{2}\left[\left(\frac{2\sigma_x - \sigma_y}{3} - \alpha_x\right)^2 + \left(\frac{2\sigma_y - \sigma_x}{3} - \alpha_y\right)^2 + \left(\frac{\sigma_x + \sigma_y}{3} + \alpha_z\right)^2\right] = \left(\sigma^{yield}\right)^2. \tag{1.27}$$

1.2.1 Isotropic linear hardening

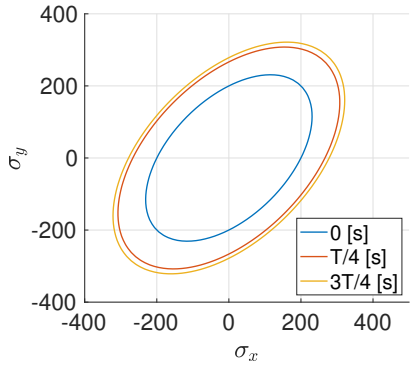

(a) One cycle in plane strain state

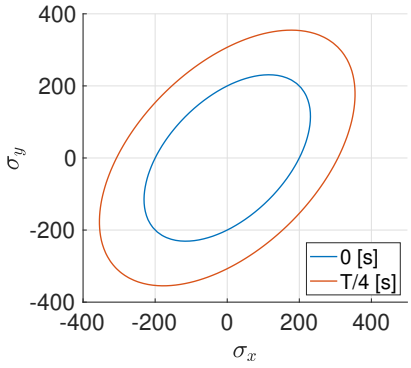

(b) One cycle in plane stress state

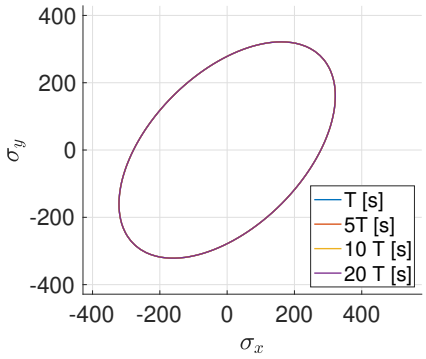

(c) Several cycles in plane strain state

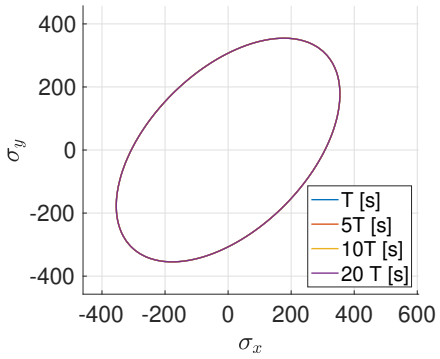

(d) Several cycles in plane stress state

Figure 5: Evolution of the yield surface over one or several cycles in the case of an isotropic linear hardening model. The results are represented either in plane strain or plane stress in the stress space defined in [MPa].

For the isotropic hardening model, as shown in Fig. 5a and 5b, the center of the yield surface is in both cases fixed and its dimensions monotonically increase. This is due to the fact that the model does not include any backstress whereas the evolution of the dimensions is directly linked to the rise of the yield stress of the linear hardening shown in Fig. 2c and 2d. Indeed, in the plane strain state, the first large yield stress increment in T/4 leads to a strong growth of the yield surface while the second one in 3T/4 induces a smaller increase. The same observation can be established in the plane stress state except that there is only one yield stress increment in T/4.

Furthermore, the geometric interpretation allows to understand the asymptotic behaviour of the model when the number of cycles tends to infinity. Since the maximal admissible surface stress $t_{\max}$ is fixed, the yield surface grows until reaching a limit surface such that there is no hardening and plasticity anymore. To show this behaviour, one can study the evolution of the yield surface considering several cycles to illustrate the asymptotic behaviour as shown in Fig. 5c and 5d. In both plane states, the limit is reached after the first period and thus after 3T/4 [s] for the plane strain state and after T/4 [s] for the plane stress state.

1.2.2 Perfectly plastic

As explained previously, the perfectly plastic case does not allow to model the hardening. Therefore, its representation in the stress space is only reduced to the initial yield surface before fracture.

1.2.3 Kinematic linear hardening

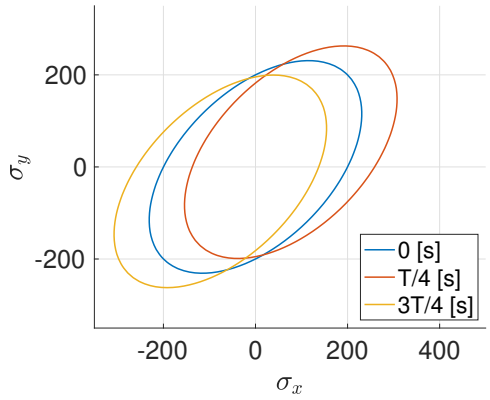

(a) One cycle in plane strain state

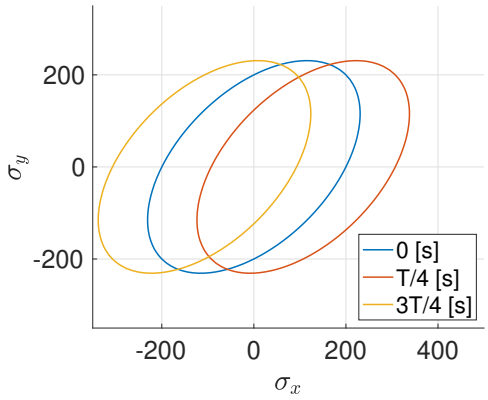

(b) One cycle in plane stress state

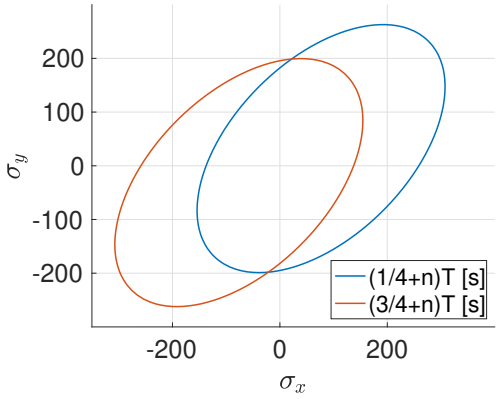

(c) Several cycles in plane strain state

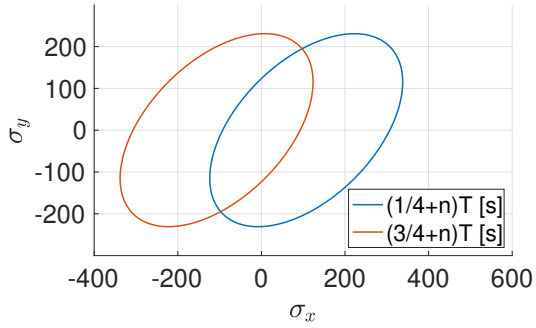

(d) Several cycles in plane stress state

Figure 6: Evolution of the yield surface over one or several cycles in the case of a kinematic linear hardening model. The results are represented either in plane strain or plane stress in the stress space defined in [MPa].

By contrast to the isotropic case, the kinematic model is such that the yield surface presents a moving center and fixed dimensions as shown in Fig. 6a and 6b. One more time, these characteristics can be explained by the yield stress and the equivalent backstress evolutions respectively shown in Fig. 3c - 3d and 3e - 3f. First, the yield stress is in both cases constant and therefore the dimensions remains unchanged. Then, both variations of the equivalent backstress $\overline{\alpha}$ in T/4 and 3T/4 [s] explain the successive translation of the center.

Moreover, given that the backstress plateau value is constant over the time, the center is successively shifted in tension and in compression by a same distance and direction. This anti-symmetric behaviour with respect to the center of the stress space allows to understand the evolution of the equivalent plastic strain shown in Fig. 3a and 3b. Indeed, this variable presents the same increments in compression and tension over the entire loading time. In this case, there is no limit surface but only successive translation of the yield surface between both yield surfaces in (1/4+n)T and (3/4+n)T shown in Fig. 6c and 6d. Hence, the equivalent plastic strain keeps increasing until the loading stops.

1.2.4 Mixed linear hardening

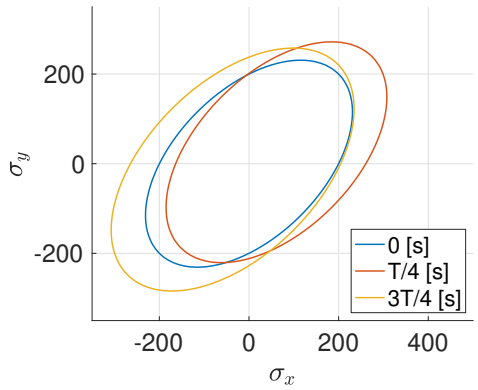

(a) One cycle in plane strain state

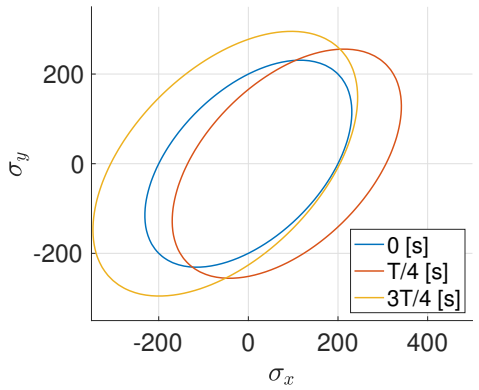

(b) One cycle in plane stress state

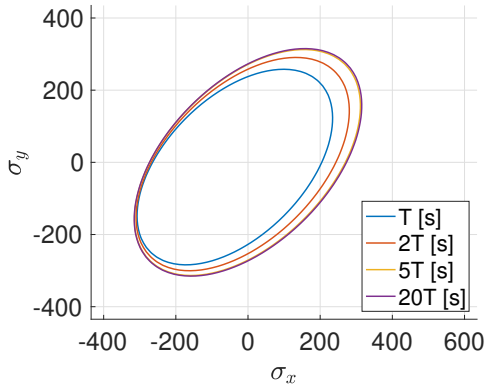

(c) Several cycles in plane strain state

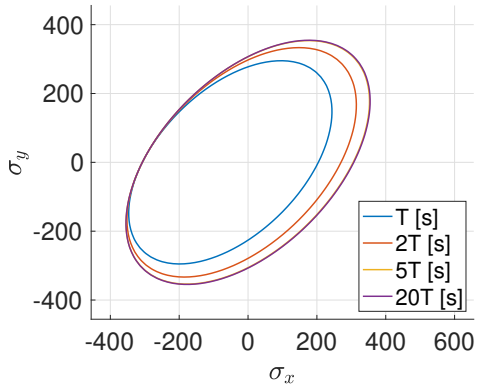

(d) Several cycles in plane stress state

Figure 7: Evolution of the yield surface over one or several cycles in the case of a mixed linear hardening model. The results are represented either in plane strain or plane stress in the stress space defined in [MPa].

Finally, the evolution of the yield surface for a mixed hardening model over a period, in Fig. 7a and 7b, is a combination of the two previous models. Indeed, the yield surface center is moving like the kinematic model and the dimensions increase like the isotropic one. However, the equivalent backstress plateau value strongly decreases over the time. As a consequence, the translation of the center is not anti-symmetric anymore as in the kinematic case. The center oscillates around the origin of the stress space with a decreasing amplitude until it converges to the origin. Indeed, considering the limit cases in Fig. 7c and 7d, it can be noticed that the yield surface ends up by converging to a limit surface whose center corresponds to the origin. These limit cases are reached after around 5 cycles for both plane states.

1.2.5 Shakedown

As explained in Sections 1.2.1 and 1.2.4, the isotropic and mixed hardening models tends to reach a limit surface after a sufficient number of cycles. Once this extreme case is reached, the stress state always belongs to the hyper-volume defined by this limit surface and the effective plastic strain remains constant. Thus, it is theoretically possible to load and unload infinitely the material without changing the yield stress and the plastic deformation. However, it is good to keep in mind that the fatigue effects, not taken into account in this study, have also a strong influence if the number of cycles becomes important. The extreme case is called shakedown effect and can be illustrated by considering the stress-strain curve $\sigma_x - \varepsilon_x$. As shown in Fig. 8a and 8b for the isotropic case and in Fig. 8c and 8d for the mixed hardening, the loading-unloading ends up by staying on the same elastic curve revealing that the limit yield surface is reached.

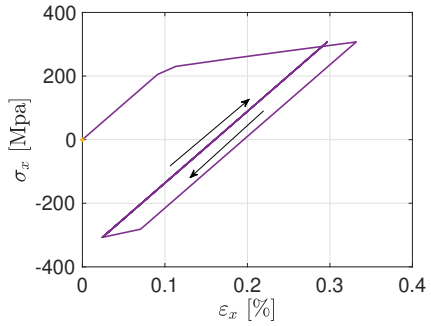

(a) Three cycles in plane strain state

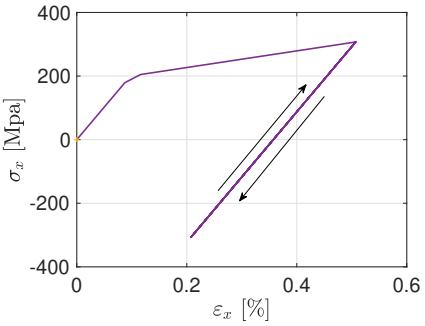

(b) Three cycles in plane stress state

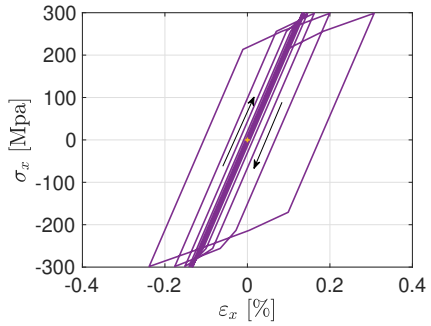

(c) Twenty cycles in plane strain state

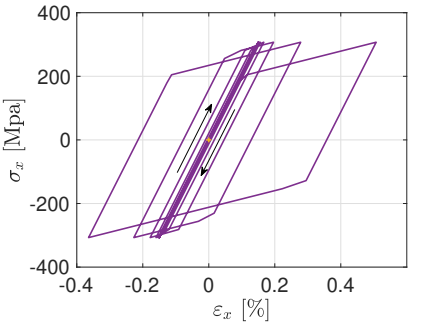

(d) Twenty cycles in plane stress state

Figure 8: Evolution of the stress-strain curve for the isotropic hardening with 3 cycles of 5 seconds (top figures) and the mixed hardening for 20 cycles of 5 seconds (bottom figures).

Conversely, the kinematic model does not allow to represent this effect as illustrated in Fig. 9a and 9b. In this case, the strain-stress state ends up by following a loop which translates a dissipative behaviour and thus a non-elastic process.

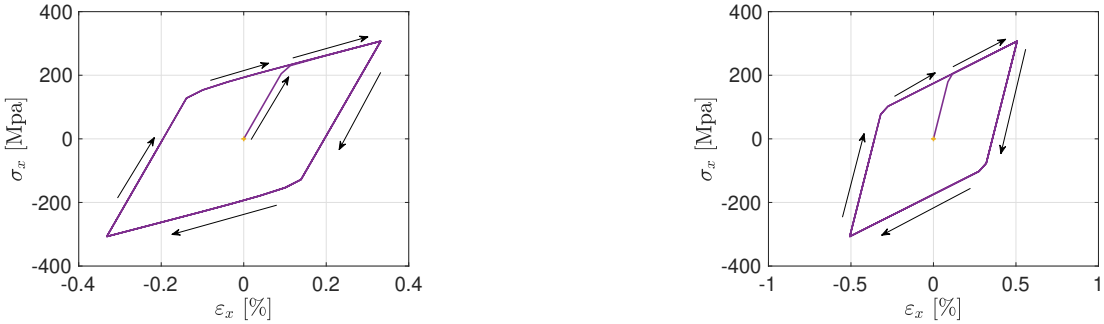

(a) Plane strain state

(b) Plane stress state

Figure 9: Stress strain curve for the kinematic hardening with 3 cycles of 5 seconds.

1.2.6 Bauschinger effect

The kinematic and mixed models allow to illustrate the Bauschinger effect. Indeed, due the displacement of the center of the yield surface, the plasticity during the reverse loading can be reached for an equivalent stress lower than the final one of the previous loading. That can be observed in Fig. 3c and 3d for the kinematic case and in Fig. 4c and 4d for the mixed model. Conversely, for the isotropic hardening in Fig. 2c and 2d, plasticity is only reached once the equivalent stress is equal to the final value of the preceding loading. Hence, there is no Bauschinger effect for this model.

1.2.7 Equivalent stress and equivalent backstress in plane strain

Based on the geometric interpretation, it is now possible to understand the evolution of the equivalent stress and backstress in plane strain. Focusing on the evolution of the stress component σ_y over the time, Fig. 2c, 3c and 4c show that its rate increases at each entry in plasticity. To explain this observation, it is good to remind that when a material undergoes plastic deformation in one direction, its stiffness decreases in the same direction. As a consequence, the y-direction, remaining undeformed, takes most of the loading during the plastic deformation of the other directions. Thus its stress rate strongly increases.

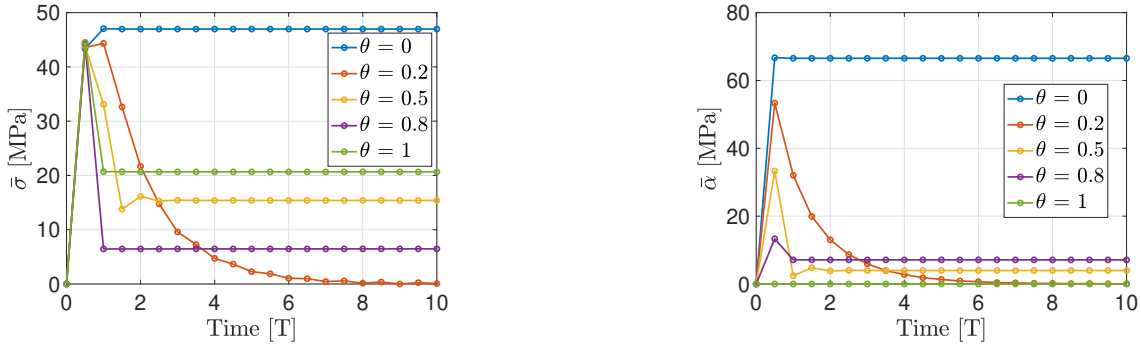

(a) Equivalent stress $\bar{\sigma}$ for different θ

(b) Equivalent backstress $\bar{\alpha}$ for different θ

Figure 10: Evolution of the equivalent stress and equivalent backstress over time for different values of the parameter θ

Thereby, it implies a phase shift between the equivalent stress and the surface traction such that $\overline{\sigma}$ can be non zero when $t(t) = 0$ [MPa]. To understand this behaviour, it seems useful to study the evolution of the equivalent stress when $t = 0$ [MPa] in plane strain for different θ values as shown in the Fig. 10a. First, regarding the kinematic hardening ($\theta = 0$), the limit value is directly reached in T/2 [s]. Once the first hardening is done, the symmetric evolution of the yield surface regarding the origin induces a constant non zero stress at each zero surface traction. Then, concerning the isotropic and mixed cases, there is a stagnation of the equivalent stress value once the limit surface is reached. This seems logical since, once there is no hardening, the phase shift between σ_x and σ_y remains constant which allows to get a constant σ_y for $t = 0$ [MPa].

In the considered model ($\theta = 0.2$), $\bar{\sigma}$ tends to a zero value for $t = 0$ [MPa] such that there is no residual stress. However, it is important to note that this is only the case for the values of θ between 0 and 0.5 as shown in Fig. 10b. Its final value is directly linked to the asymptotic value of the equivalent backstress $\bar{\alpha}$. Indeed, if the final ellipse is not centered at the origin i.e. if $\bar{\alpha}$ is non zero at the limit case, there is a residual stress.

Note that the plane stress has not been considered in this section since, as seen previously, this case corresponds to a simple traction-compression with $\bar{\sigma} = |\sigma_x|$ such that $\bar{\sigma} = 0$ for $t = 0$ [MPa].

1.2.8 Influence of a reverse loading

The symmetry of the yield surface and of the loading allow to claim that a reverse loading, i.e. compression before traction, does not influence the relevant variables. Only the stress, strain and backstress components present a change of sign.

1.3 Equivalent plastic strain

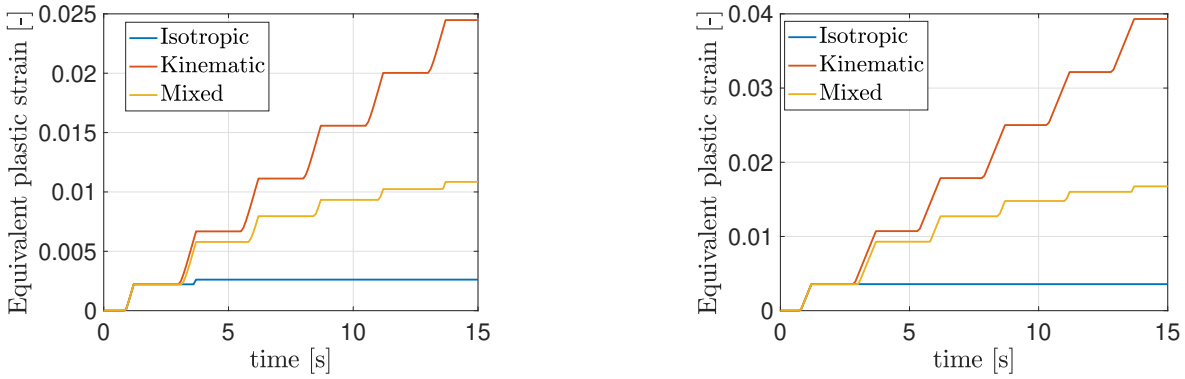

(a) Plane strain state

(b) Plane stress state

Figure 11: Equivalent plastic strain for the 3 different hardening models with 3 cycles of 5 seconds.

Now that the different models are introduced, it seems relevant to focus on the equivalent plastic strain. As it can be seen in Fig. 11a and 11b, the growth of the equivalent plastic strain is more important with the mixed and kinematic models compared to the isotropic case. Moreover, it is important to note that the first increment of the plastic strain is the same whatever the hardening

model once the surface traction reaches $t_{\max}$ for the first time. On one hand, since the material is initially virgin, the yield stress is the initial one and the backstress is zero whatever the model. Therefore, the different types of hardening have the same yield hyper-surface and the plasticity begins at the same time. One the other hand, the rate of the plastic strain during this first increment is expressed as follows:

$$\dot{\bar{\varepsilon}}^p = \sqrt{\frac{2}{3}}\lambda, \tag{1.28}$$

where λ depends on the type of hardening :

$$\lambda = \frac{N_{kl}D_{kl}}{1+\frac{h}{3G}} \quad \text{with} \quad h = h_i + h_k \quad \text{and} \quad \begin{cases} h_i = \theta h, \\ h_k = (1-\theta)h. \end{cases} \tag{1.29}$$

The isotropic ($\theta = 1$), the kinematic ($\theta = 0$) and the mixed ($\theta = 0.2$) models present the same hardening parameter h and shear modulus G. Furthermore, the direction of the plastic flow N_{kl} is also the same since the yield surface and the surface traction are the same and the strain rate is equal to the elastic one given that there is no plastic deformation yet, i.e. $D_{kl} = D^e_{kl}$ and $D^p_{kl} = 0$. Therefore, the first plastic increment occurs at the same time whatever the hardening model and presents the same rate, which leads to the same plastic increment for all hardening models.

1.4 Plastic dissipation

Finally, one can focus on the plastic dissipation. Usually, the energy is dissipated into two parts: 95% of heat and 5% to to reorganize the system. The plastic dissipation rate is calculated as follows:

$$\mathcal{D} = \sigma_{ij} \cdot D^p_{ij} = \boldsymbol{\sigma} : \mathbf{D}^p. \tag{1.30}$$

Using the flow rule, the plastic dissipation rate can be re-written as:

$$\mathcal{D} = \lambda \sigma_{ij} N_{ij}. \tag{1.31}$$

Moreover, the flow intensity can be linked to the equivalent plastic strain rate such that:

$$\dot{\bar{\varepsilon}}^p = \sqrt{\frac{2}{3}}\lambda \quad \longrightarrow \quad \lambda = \dot{\bar{\varepsilon}}^p \sqrt{\frac{3}{2}}. \tag{1.32}$$

Therefore, substituting λ in the equation of the plastic dissipation rate, it comes:

$$\mathcal{D} = \dot{\bar{\varepsilon}}^p \sqrt{\frac{3}{2}} \sigma_{ij} N_{ij}. \tag{1.33}$$

The plastic dissipation is defined as the energy dissipated by the plastic deformation and therefore equal to the inelastic work, W_{in}. Thus, by time-integration of the plastic dissipation rate, it comes:

$$W_{in} = \int \mathcal{D}\, dt = \int \dot{\bar{\varepsilon}}^p \sqrt{\frac{3}{2}} \sigma_{ij} N_{ij}\, dt. \tag{1.34}$$

Eq. 1.34 allows to compute the plastic dissipation based on the results of the simulations for 3 cycles of 5 seconds as shown in Fig. 12a and 12b.

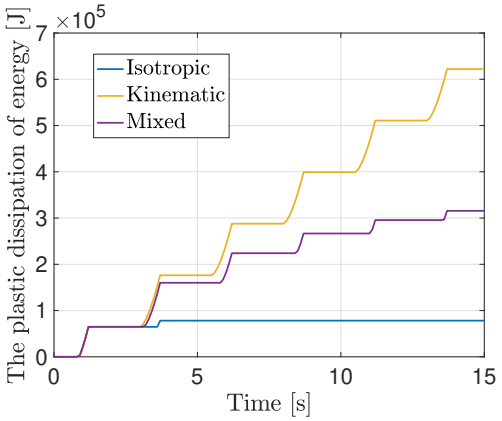

(a) The energy dissipated in plasticity for 3 cycles of 5 seconds in plane strain.

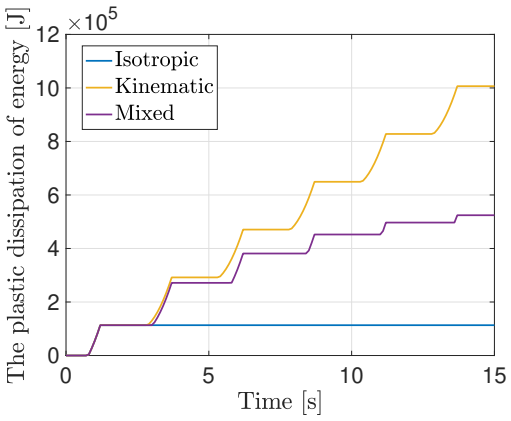

(b) The energy dissipated in plasticity for 3 cycles of 5 seconds in plane stress.

Figure 12: Evolution of the plastic dissipation in plane strain and plane stress.

As expected, the evolution of the plastic dissipation is heavily linked to the evolution of the plastic strain such that plastic dissipation is only induced for a non zero equivalent plastic strain rate. Thus, an elastic process is well conservative and reversible.

Moreover, one can note that the kinematic model leads to larger dissipation than both other models at the end of the loading. As seen previously, this model leads to constant plastic strain increments until the end of the loading due to the yield surface evolution with constant dimensions. Therefore, the energy dissipation increases until the end of the loading. Conversely, both isotropic and mixed models lead to a convergence of the yield surface and thus, the equivalent plastic strain stops increasing so does the plastic dissipation.

Part 2 - Elasto-plastic behavior with non-linear hardening

In this second part, the non-linear kinematic hardening law described by Armstrong Frederick's evolution law of the backstress tensor will be studied. First of all, the dynamic recovery parameter η_k is introduced and its influence on the different relevant variables is analyzed. Then, the behaviour of the cube under several loading/unloading cycles is studied using the hardening law set in one case to purely kinematic and on the other case to mixed with isotropic hardening.

2.1 The dynamic recovery parameter η_k

The evolution law of the backstress tensor given by Melan and Prager possess a flaw from a physical point of view. Indeed, their equation suppose that $\dot{\boldsymbol{\alpha}}$ evolves linearly with the plastic strain rate $\mathbf{D}^p$. Therefore, the material would remain in its exact stress state if the load is removed. From a physical point of view, it is hard to imagine that the material would not relax under a no stress state. The evolution law for the backstress tensor proposed by Armstrong and Frederick has for purpose to introduce a non-linear dynamic recovery term which represents a fading memory effect. In other words, this new term mimics the relaxation of the material as well as its resistance to a plastic deformation which allows to represent better the Bauschinger effect. The new evolution equation is given as follows:

$$\dot{\alpha}_{ij} = \frac{2}{3}\, h_k\, D^p_{ij} - \underbrace{\eta_k\, \dot{\bar{\varepsilon}}^p\, \alpha_{ij}}_{\text{Dynamic recovery term}}, \tag{2.35}$$

where the dynamic recovery term introduces the new parameter η_k. As it can be seen on Eq. 2.35, this new parameter has for purpose to determine the intensity of dynamic fading memory effect. Furthermore, one can easily observe that η_k is dimensionless in order to conserve the dimension of the backstress tensor.The general form of an internal parameter evolution law is given by:

$$\dot{\mathbf{q}}^{(k)} = \lambda \times r^{(k)}(\boldsymbol{\sigma}, \mathbf{q}), \tag{2.36}$$

where λ is defined as the flow intensity and $r^{(k)}$ depends on the hardening model used to describe plasticity. In the case of the evolution law of $\boldsymbol{\alpha}$, given the fact that the hardening model is non-linear, the expression of $r^{(k)}$ gives:

$$\dot{\alpha}_{ij} = \lambda \left(\frac{2}{3} h_k N_{ij} - \eta_k \sqrt{\frac{2}{3}} \alpha_{ij} \right). \tag{2.37}$$

This equation can be recovered from Eq. 2.35 since $D^p_{ij} = \lambda\, N_{ij}$ where N_{ij} is the unit normal tensor in the plastic flow direction and $\dot{\bar{\varepsilon}}^p = \sqrt{\frac{2}{3}}\lambda$.

2.2 Influence of η_k on the asymptotic backstress α_{ij}^u

In order to understand better the effect of the dynamic recovery parameter on $\boldsymbol{\alpha}$, it is interesting to compute the asymptotic value of the backstress tensor. First, it is considered that the plastic multiplier is strictly positive $\lambda > 0$ or in other words the material is undergoing a plastic deformation. The asymptotic value α_{ij}^u, i.e the value such that $\dot{\alpha}_{ij} = 0$, can be retrieved from the following mathematical expression:

$$\dot{\alpha}_{ij} = \frac{2}{3} h_k D_{ij}^p - \eta_k \dot{\bar{\varepsilon}}^p \alpha_{ij}^u = \underbrace{\frac{2}{3} h_k \lambda N_{ij}}_{(a)} - \underbrace{\eta_k \sqrt{\frac{2}{3}} \lambda \alpha_{ij}^u}_{(b)} = 0. \tag{2.38}$$

The former equation describes an equilibrium of forces. Indeed, the first linear term (a) tends to move the center of the yield surface away from its initial position whereas the second non-linear term (b) tends to bring back the center to its initial position. When the asymptotic value α_{ij}^u is reached, these forces are balancing each other and the center of the yield surface does not move anymore. From the Eq. 2.38, the asymptotic value of $\boldsymbol{\alpha}$ can easily be computed:

$$\alpha_{ij}^u = \sqrt{\frac{2}{3}} \frac{h_k N_{ij}}{\eta_k}. \tag{2.39}$$

In addition to that, by using the general definition of the equivalent backstress $\overline{\alpha}$ as well as the former result, the asymptotic value of the latter can be found as:

$$\overline{\alpha}^u = \sqrt{\frac{3}{2} \alpha_{ij}^u \alpha_{ij}^u} = \frac{h_k}{\eta_k}. \tag{2.40}$$

From this equation, the influence of η_k can be easily deduced. Indeed, if the value of the dynamic recovery parameter increases, the asymptotic equivalent backstress decreases. Physically, this means that the yield surface tends to stay at its initial position.

2.3 Influence of η_k on the generalized plastic modulus H^p

During a plastic deformation, the resistance that a material oppose to this deformation can be characterized by the generalized plastic modulus H^p. Therefore, it is interesting to find the influence of the dynamic recovery parameter on it. First of all, the general expression of H^p can be derived from the consistency equation which is stated as follows:

$$\dot{f} = \frac{\partial f}{\partial \sigma_{ij}} \, \dot{\sigma}_{ij} + \frac{\partial f}{\partial \mathbf{q}^{(k)}} * \dot{\mathbf{q}}^{(k)} = 0. \tag{2.41}$$

Then, using Eq. 2.36, the expression of the former equation can be developed as:

$$\dot{f} = \frac{\partial f}{\partial \sigma_{ij}} \, \dot{\sigma}_{ij} + \frac{\partial f}{\partial \mathbf{q}^{(k)}} * \lambda \, r^{(k)}(\boldsymbol{\sigma}, \mathbf{q}) = 0, \tag{2.42}$$

where the generalized plastic modulus can be defined as:

$$H^p = -\frac{\partial f}{\partial \mathbf{q}^{(k)}} * r^{(k)}(\boldsymbol{\sigma}, \mathbf{q}). \tag{2.43}$$

Hence, from the consistency equation, one can finally deduce that

$$\frac{\partial f}{\partial \sigma_{ij}}\dot{\sigma}_{ij} - \lambda\, H^p = 0 \quad \Leftrightarrow \quad H^p = \frac{1}{\lambda}\frac{\partial f}{\partial \sigma_{ij}}\dot{\sigma}_{ij}. \tag{2.44}$$

Now, the final step is to find a way to express $\frac{\partial f}{\partial \sigma_{ij}}\dot{\sigma}_{ij}$ in terms of η_k. Since the different internal variables of the problems are known as well as their evolution laws, the left term of the Eq. 2.44 can be developed by starting once again from the consistency equation. Indeed, the latter can be expressed as:

$$\dot{f} = \frac{\partial f}{\partial \sigma_{ij}}\dot{\sigma}_{ij} + \frac{\partial f}{\partial \alpha_{ij}}\dot{\alpha}_{ij} + \frac{\partial f}{\partial \sigma_y}\dot{\sigma}_y = 0,$$

$$\Leftrightarrow \quad \frac{\partial f}{\partial \sigma_{ij}}\dot{\sigma}_{ij} = -\frac{\partial f}{\partial \alpha_{ij}}\dot{\alpha}_{ij} - \frac{\partial f}{\partial \sigma_y}\dot{\sigma}_y. \tag{2.45}$$

The Eq. 2.45 introduces new unknowns that must be defined. For starter, the derivative of the yield function with respect to the stress tensor can be retrieved by considering the Von Mises yield criterion

$$f = \overline{\sigma}^{VM} - \sigma_y = \sqrt{\frac{3}{2}\left(s_{ij} - \alpha_{ij}\right)\left(s_{ij} - \alpha_{ij}\right)} - \sigma_y \leq 0. \tag{2.46}$$

Deriving this expression with respect to σ_{ij}, which is equivalent to deriving it with respect to the deviatoric tensor s_{ij}, one obtains:

$$\frac{\partial f}{\partial \sigma_{ij}} = \frac{\partial f}{\partial s_{ij}} = \sqrt{\frac{3}{2}}\frac{s_{ij} - \alpha_{ij}}{\sqrt{\left(s_{kl} - \alpha_{kl}\right)\left(s_{kl} - \alpha_{kl}\right)}}. \tag{2.47}$$

If associated plasticity is assumed, i.e the plastic flow potential g is equal to the yield function f, one can conclude that its derivative is in the direction of the plastic flow. In addition to that, it is possible to observe that the following term

$$\frac{s_{ij} - \alpha_{ij}}{\sqrt{\left(s_{kl} - \alpha_{kl}\right)\left(s_{kl} - \alpha_{kl}\right)}}. \tag{2.48}$$

is in the form of a quantity divided by its norm such that we can define it as the unit normal in the direction of the plastic flow N_{ij}. Thus, the final expression of the Eq. 2.47 is:

$$\frac{\partial f}{\partial \sigma_{ij}} = \sqrt{\frac{3}{2}}N_{ij}. \tag{2.49}$$

It is also important to notice that the derivative of the yield function f with respect to the backstress tensor α_{ij} is the opposite of the derivative with respect to σ_{ij}:

$$\frac{\partial f}{\partial \alpha_{ij}} = \sqrt{\frac{3}{2}}\frac{\alpha_{ij} - s_{ij}}{\sqrt{\left(s_{kl} - \alpha_{kl}\right)\left(s_{kl} - \alpha_{kl}\right)}} = -\frac{\partial f}{\partial \sigma_{ij}} = -\sqrt{\frac{3}{2}}N_{ij}. \tag{2.50}$$

From the Eq. 2.50, it can be seen that the backstress tensor act in the opposite direction of the plastic flow. This observation is physically correct since the backstress tensor must bring back the center of the yield surface after hardening. Indeed, if they were working in the same direction, it would imply that the backstress works in snowball effect with the plastic flow or in other words, the deformation of the material is amplified even more. In addition to that, the term $\frac{\partial f}{\partial \sigma_y}$ is easily retrieved from Eq. 2.46 as:

$$\frac{\partial f}{\partial \sigma_y} = -1. \tag{2.51}$$

Using the results of Eq. 2.50 and Eq. 2.51, the consistency condition can now be expressed as:

$$\frac{\partial f}{\partial \sigma_{ij}} \dot{\sigma}_{ij} = \sqrt{\frac{3}{2}} N_{ij}\, \dot{\alpha}_{ij} + \dot{\sigma}_y. \tag{2.52}$$

This expression can be particularized for a non-linear mixed hardening in order to determine the most general expression. Indeed, due to the new expression of the hardening coefficient, one can easily switch from mixed to purely isotropic/kinematic hardening by changing the value of θ. The expression of the evolution law for the yield stress for the linear isotropic and non-linear isotropic cases are respectively given by:

$$\dot{\sigma}_y = \begin{cases} h_i \dot{\overline{\varepsilon}}^p = h_i \sqrt{\frac{2}{3}} \lambda, \\ h_i \dot{\overline{\varepsilon}}^p \exp\left(-\frac{h_i \overline{\varepsilon}^p}{\sigma_y^\infty - \sigma_y^0} \right) = h_i \sqrt{\frac{2}{3}} \lambda \exp\left(-\frac{h_i \overline{\varepsilon}^p}{\sigma_y^\infty - \sigma_y^0} \right). \end{cases} \tag{2.53}$$

In the case of a linear isotropic hardening of the yield stress, one obtains:

$$\begin{aligned} \frac{\partial f}{\partial \sigma_{ij}} \dot{\sigma}_{ij} &= \sqrt{\frac{3}{2}} N_{ij} \cdot \lambda \left(\frac{2}{3} h_k N_{ij} - \eta_k \sqrt{\frac{2}{3}} \alpha_{ij} \right) + \lambda \sqrt{\frac{2}{3}} h_i, \\ &= \lambda \left(\sqrt{\frac{2}{3}} h_k - \eta_k N_{ij} \alpha_{ij} + \sqrt{\frac{2}{3}} h_i \right), \\ &= \lambda \left(\sqrt{\frac{2}{3}} \left(h_k + h_i \right) - \eta_k N_{ij} \alpha_{ij} \right), \end{aligned} \tag{2.54}$$

whereas for the non-linear isotropic hardening of the yield stress, one can directly deduce the needed expression by analogy :

$$\frac{\partial f}{\partial \sigma_{ij}} \dot{\sigma}_{ij} = \lambda \left(\sqrt{\frac{2}{3}} \left(h_k + h_i \exp\left(-\frac{h_i \overline{\varepsilon}^p}{\sigma_y^\infty - \sigma_y^0} \right) \right) - \eta_k N_{ij} \alpha_{ij} \right). \tag{2.55}$$

By using Eq. 2.54 and Eq. 2.55, it is possible to obtain the following final equations expressing the generalized plastic modulus H^p for both cases:

$$H^p = \begin{cases} \sqrt{\frac{2}{3}}\left(h_k + h_i\right) - \eta_k N_{ij}\alpha_{ij}, & \textbf{linear isotropic hardening} \\ \sqrt{\frac{2}{3}}\left(h_k + h_i \exp\left(-\frac{h_i \bar{\varepsilon}^p}{\sigma_y^\infty - \sigma_y^0}\right)\right) - \eta_k N_{ij}\alpha_{ij}. & \textbf{non-linear isotropic hardening} \end{cases}$$

This equation can also be written in tensor form :

$$H^p = \begin{cases} \sqrt{\frac{2}{3}}(h_k + h_i) - \eta_k \frac{(\mathbf{s}-\boldsymbol{\alpha}) : \boldsymbol{\alpha}}{\sqrt{(\mathbf{s}-\boldsymbol{\alpha}) : (\mathbf{s}-\boldsymbol{\alpha})}}, \\ \sqrt{\frac{2}{3}}\left(h_k + h_i \exp\left(-\frac{h_i \bar{\varepsilon}^p}{\sigma_y^\infty - \sigma_y^0}\right)\right) - \eta_k \frac{(\mathbf{s}-\boldsymbol{\alpha}) : \boldsymbol{\alpha}}{\sqrt{(\mathbf{s}-\boldsymbol{\alpha}) : (\mathbf{s}-\boldsymbol{\alpha})}}. \end{cases} \tag{2.56}$$

The influence of the dynamic recovery parameter on the generalized plastic modulus can be determined by observing the behaviour of the term $(\mathbf{s}-\boldsymbol{\alpha}) : \boldsymbol{\alpha}$ at critical points of one cycle. Indeed, as it corresponds to the direction of the normal during the loading, its orientation will indicate the direction of the effect of the recovery term. This phenomenon can be illustrated using Fig. 13 and 14. Indeed, the material is first subjected to a traction which leads to a translation of the yield surface as it can be seen on point 1 of Fig. 13 and the backstress is in the same direction as the deviatoric stress. Then, when the load is removed, s slowly decreases due to the elastic recovery process but $\boldsymbol{\alpha}$ keeps pointing to the same direction since it does not evolve during plasticity. This phenomenon is also represented in the next section on Fig. 19, indeed it can be seen that $\boldsymbol{\alpha}$ increases and afterwards remains constant when the loading is removed. During compression, the backstress decreases since the yield surface is brought back in the other direction. Therefore, after a small period of time, $\boldsymbol{\alpha}$ starts to point in the same direction as $\mathbf{s}$ as it show on point 3 of Fig. 14. Finally, when the load is removed, the yield surface slowly tries to come back to its original position due to the elastic recovery while the back stress still points in the same direction. Using Fig. 19, one can see that during compression the backstress decreases and the moment it becomes negative correspond to its change of direction and alignment with $\mathbf{s}$.

From the expression of generalized plastic modulus in Eq. 2.56, it can be concluded that the dynamic recovery parameter η_k plays a fundamental role regarding the hardening of the material. Indeed, as the value of η_k increases, the effect of the recovery term becomes more consequent which implies that the material will resist more to the hardening effect. A simple analogy can be made by thinking of η_k as the stiffness of a spring, if a force is applied to it the stiffness will reduce the effect of the deformation as it makes the spring more rigid. Two limit cases can be deduced:

1. The material has no stiffness, therefore the hardening becomes purely linear without any recovery. and in this case η_k must be equal to 0.

2. On the contrary, if the stiffness is too high, i.e if $\eta_k >>$, the recovery is very high and the yield surface will not move. For a purely kinematic hardening case, this corresponds to recovering a perfectly plastic model as described previously.

It is also important to remember that one of the main purpose of the non-linear kinematic hardening is to represent better the Bauschinger effect. Thus, one can observe that the dynamic recovery term acts to reduce this effect by bringing back the yield surface to its initial position. In the second limit case, the Bauschinger effect is completely cancelled. In order to visualize the effect of the dynamic recovery parameter on the plastic generalize plastic modulus, one can represent the evolution of the yield surface in Haigh Westergaard's space when the material is put under a uni-axial tension in the following way:

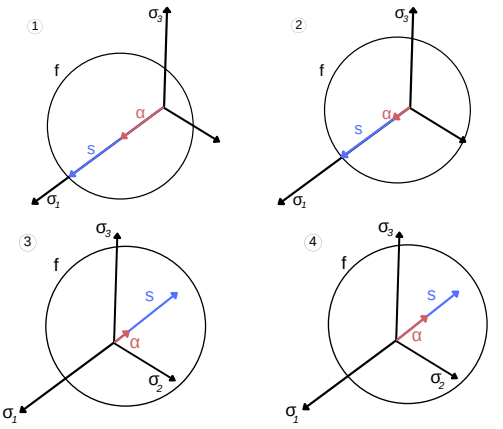

Figure 13: Representation of the backstress α and the deviatoric stress s in Haigh Westergaard coordinate system in traction.

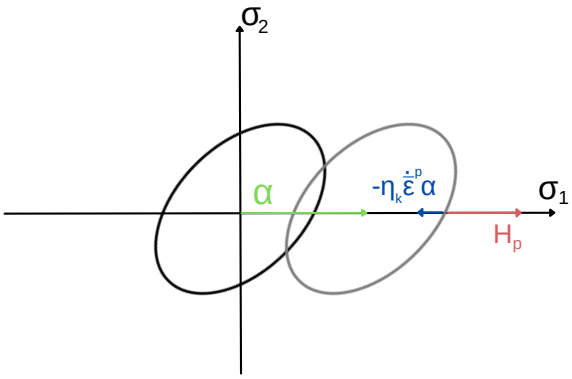

Figure 14: Effect of the dynamic recovery parameter on the plastic generalize plastic modulus in Haigh Westergaard.

2.4 Purely kinematic non-linear hardening

The study of the behaviour of the cube under loading cycles starts first by considering a purely kinematic non-linear hardening law. In this case, as it was explained previously, the yield surface is only undergoing translations. First of all, the evolution of the equivalent plastic strain for different maximum values of the loading is represented on Fig. 15.

As it can be seen, the load t_{max} does not have a particular effect on the general behaviour of $\overline{\varepsilon}^p$ beside increasing its value as the load also increases. In order to bring more information about what happens during tension and compression, it is interesting to find a relation that relates the evolution of the backstress tensor α_{ij} as a function of the effective plastic strain $\overline{\varepsilon}^p$. In this case, the components of the backstress tensor must be chosen such that $\overline{\alpha} = |\alpha|$. In other words,

$$\alpha_{ij} \cdot \alpha_{ij} = \frac{2}{3}\alpha^2. \tag{2.57}$$

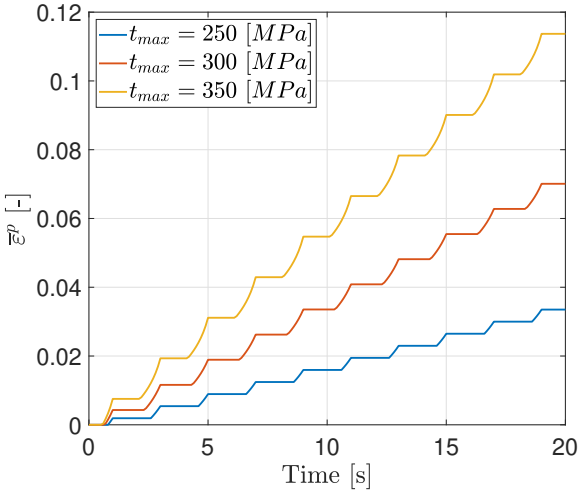

Figure 15: Evolution of $\overline{\varepsilon}^p$ in the case of a purely kinematic non-linear hardening law.

In the case of uni-axial loading, the Eq. 2.35 can be simplified. Indeed, due to Eq. 2.57 and Eq. 0.22 $\alpha_{xx} = \frac{2}{3}\alpha$ and posing $\varepsilon^p_{xx} = \varepsilon^p$, this equation can be rewritten as:

$$\dot{\alpha} = h_k \dot{\varepsilon}^p - \eta_k \dot{\bar{\varepsilon}}^p \alpha. \tag{2.58}$$

By definition, $\bar{\varepsilon}^p = |\varepsilon^p_{xx}| = |\varepsilon^p|$ and thus, traction and compression have to be considered separately. The Eq. 2.58 is a first order differential equation whose solution can be decomposed as the sum of a general and particular solution. This equation can be written as:

$$\begin{aligned} \frac{d\alpha}{dt} &= h_k \frac{d\varepsilon^p}{dt} - \eta_k \frac{d\,|\varepsilon^p|}{dt}\alpha \\ &= h_k \frac{d\varepsilon^p}{dt} \mp \eta_k \frac{d\varepsilon^p}{dt}\alpha \\ &= (h_k \mp \eta_k \alpha)\, \frac{d\varepsilon^p}{dt}. \end{aligned} \tag{2.59}$$

By rearranging the terms, the following differential equation is obtained:

$$\frac{d\alpha}{d\varepsilon^p} \pm \eta_k \alpha = h_k. \tag{2.60}$$

The Eq. 2.60 must be solved by considering traction and compression separately. The resolution goes as follows:

Traction

In this case, the term $\dot{\varepsilon}^p$ is positive thus the equation to solve is:

$$\frac{d\alpha}{d\varepsilon^p} + \eta_k \alpha = h_k. \tag{2.61}$$

The general solution is retrieved from the homogeneous equation as follows:

$$\begin{aligned} &\frac{d\alpha}{d\varepsilon^p} + \eta_k \alpha = 0 \\ \Leftrightarrow \quad &\alpha_h(\varepsilon^p) = A \cdot \exp(-\varepsilon^p \cdot \eta_k). \end{aligned}$$

The particular solution is retrieved by inspection of the equation (2.61):

$$\alpha_p = \frac{h_k}{\eta_k}.$$

Compression

In this case, the term $\dot{\bar{\varepsilon}}^p$ is negative thus the equation to solve is:

$$\frac{d\alpha}{d\varepsilon^p} - \eta_k \alpha = h_k. \tag{2.62}$$

The general solution is retrieved from the homogeneous equation as follows:

$$\begin{aligned} &\frac{d\alpha}{d\varepsilon^p} - \eta_k \alpha = 0 \\ \Leftrightarrow \quad &\alpha_h(\varepsilon^p) = B \cdot \exp(\varepsilon^p \cdot \eta_k). \end{aligned}$$

The particular solution is retrieved by inspection of the equation (2.62):

$$\alpha_p = -\frac{h_k}{\eta_k}.$$

Therefore, the general form of the backstress evolution law with respect to the plastic strain is:

$$\alpha_h(\varepsilon^p) = C^{st} \exp(\mp\varepsilon^p \cdot \eta_k) \pm \frac{h_k}{\eta_k}. \tag{2.63}$$

Finally, since the simulations are done with a virgin material, this implies that the initial effective plastic strain is equal to 0 as well as the initial value of the backstress. Thus, the final solution is given by:

$$\alpha(\varepsilon^p) = \pm\frac{h_k}{\eta_k}(1 - \exp(\mp\eta_k \cdot \varepsilon^p)). \tag{2.64}$$

From this expression, one can observe that if the deformation increases a lot, the analytical expression of the backstress tends to an asymptotic value. Indeed, if ε^p increases a lot, the exponential term tends to zero and thus the asymptotic value is given by:

$$\alpha^u = \pm\frac{h_k}{\eta_k}. \tag{2.65}$$

This expression is the same as the one found in section 2.2 for the asymptotic equivalent backstress. In addition to that, it is possible to observe the relation between $\overline{\sigma}$ and $\overline{\varepsilon}^p$ knowing that:

$$\frac{d\overline{\sigma}}{d\overline{\varepsilon}^p} = \sqrt{\frac{3}{2}}H^p = h. \tag{2.66}$$

From this expression, it is clear that the hardening parameter is the slope of the curve $\overline{\sigma}(\overline{\varepsilon}^p)$ and thus, the evolution of the effective stress with respect to the effective plastic strain will not be linear as the hardening parameter h usually depends on the effective plastic strain $\overline{\varepsilon}^p$.

This curve can be observed for one loading/unloading cycle and for different values of t_{max} in Fig. 16. From this figure, it is clear that this curve does not represent a closed cycle in the stress-strain space $\overline{\sigma} - \overline{\varepsilon}^p$. This can be explained by the fact that the effective plastic strain should never decreases such that if plasticity is reached, there is no sense to look for a close cycle in this space. Indeed, in plasticity, the material will undergo a permanent deformation and thus the strain can not go back to zero. One should also notice the increase of $\overline{\sigma}$ becomes slower as $\overline{\varepsilon}^p$ increases. This is due to the fact that the slope $h = h_k$ decreases with the effective plastic strain as the dynamic recovery term opposes the translation of the yield surface.

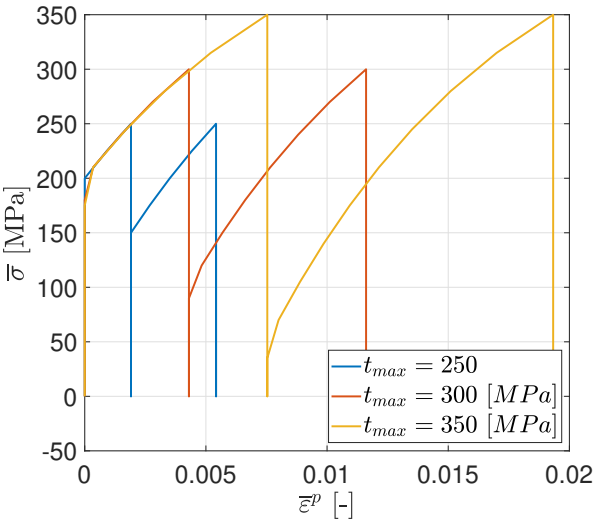

Figure 16: Evolution of the equivalent stress with respect to the effective plastic strain for different values of the load t_{max}.

It is also possible to find an upper bound for the equivalent stress $\overline{\sigma} = \sqrt{3J_2}$. Starting from the expression of the latter, one can write:

$$\begin{aligned}\overline{\sigma} = \sqrt{3J_2} &= \sqrt{\frac{3}{2}s_{ij}s_{ij}} \\ &= \sqrt{\frac{3}{2}\mathbf{s}:\mathbf{s}} = \sqrt{\frac{3}{2}\left|\left|\mathbf{s}\right|\right|^2} \\ &= \sqrt{\frac{3}{2}}\left|\left|\mathbf{s}\right|\right|. \end{aligned} \tag{2.67}$$

Now, it is necessary to introduce the Von Mises equivalent stress expression in the previous equation to find the upper bound. This can simply be done by adding by adding and subtracting the backstress tensor $\boldsymbol{\alpha}$:

$$\sqrt{3J_2} = \sqrt{\frac{3}{2}}\left|\left|(\mathbf{s}-\boldsymbol{\alpha})+\boldsymbol{\alpha}\right|\right|. \tag{2.68}$$

Using the triangular inequality in this last equation, the following relation is obtained:

$$\begin{aligned}\sqrt{3J_2} &\leq \sqrt{\frac{3}{2}}\left|\left|\mathbf{s}-\boldsymbol{\alpha}\right|\right| + \sqrt{\frac{3}{2}}\left|\left|\boldsymbol{\alpha}\right|\right| \\ &\leq \sqrt{\frac{3}{2}\left(s_{ij}-\alpha_{ij}\right)\left(s_{ij}-\alpha_{ij}\right)} + \sqrt{\frac{3}{2}\alpha_{ij}\alpha_{ij}}. \end{aligned} \tag{2.69}$$

In this last equation, the terms in the right-hand side are known as they correspond respectively to the Von Mises equivalent stress and the equivalent backstress. Hence, the Eq. 2.69 becomes:

$$\sqrt{3J_2} \leq \overline{\sigma}^{VM} + \overline{\alpha}. \tag{2.70}$$

Then, using the general expression of the yield function, one can write that $\overline{\sigma}^{VM}$ is always lower than the current yield stress σ_y. Using this, the upper bound of the equivalent stress becomes:

$$\sqrt{3J_2} \ \leq \ \sigma_y + \overline{\alpha}. \tag{2.71}$$

This limit value is obtained when the asymptotic values of the yield stress and of the equivalent backstress is reached. This finally gives:

$$\sqrt{3J_2} \leq \sigma_y^u + \overline{\alpha}^u = \sigma_y^u + \frac{h_k}{\eta_k}. \tag{2.72}$$

In the case of a purely kinematic hardening, recalling that $\sigma_y^u = \sigma_y^0$, the upper bound of the equivalent stress is:

$$\overline{\sigma} = \sqrt{3J_2} \leq \sigma_y^0 + \frac{h_k}{\eta_k}. \tag{2.73}$$

Using Eq. 2.73, the expression of the asymptotic yield surface can be derived and this gives:

$$f^u = \sqrt{3J_2} - \sigma_y^0 - \frac{h_k}{\eta_k} \leq 0. \tag{2.74}$$

This surface is illustrated in Fig. 17. In this figure, it can clearly be observed that the the size of the surface remains the same as the yield stress does not evolve for a purely kinematic hardening. The asymptotic surface represented in Fig. 17 corresponds to the case of the traction. Indeed, in compression the same behaviour is obtained but in the opposite direction. Thus, this surface represents the furthest position that can be reached by the yield surface. In other words, the position of the surface during the loading will be situated between the asymptotic surface in traction and compression.

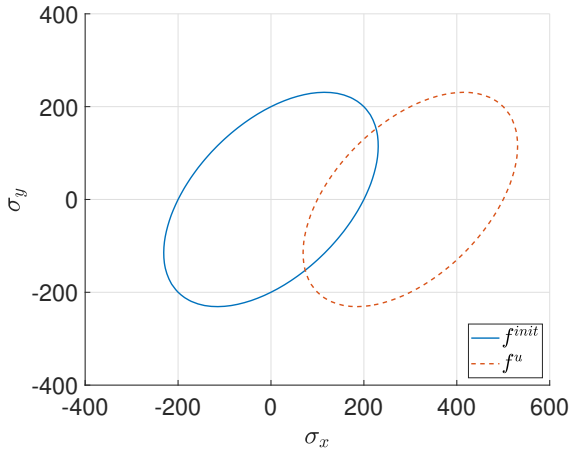

Figure 17: Initial yield surface and asymptotic yield surface in the purely kinematic case for $\eta_k = 100$

In order to even better understand the influence of the maximum load, it is important to observe numerically the behaviour of physical quantities such as the strain, the stress, the backstress and so on. Therefore, one will observe their evolution for different types of loading using an arbitrarily fixed recovery parameter $\eta_k = 100$. First of all, the focus is placed on the yield stress. In the case of the fully kinematic hardening law, the current yield stress is always equal to the initial one. Therefore, its evolution law is simply given by:

$$\dot{\sigma}_y = 0. \tag{2.75}$$

This result is in concordance with the numerical ones. Indeed, as it can be seen in Fig. 18, the yield stress does remain constant during the whole cycle. In addition to that, the evolution of the Von Mises yield stress shows is bounded to 200 [MPa] since this correspond to the initial yield. Indeed, $\overline{\sigma}^{VM}$ do not take into account the translation of the yield surface.

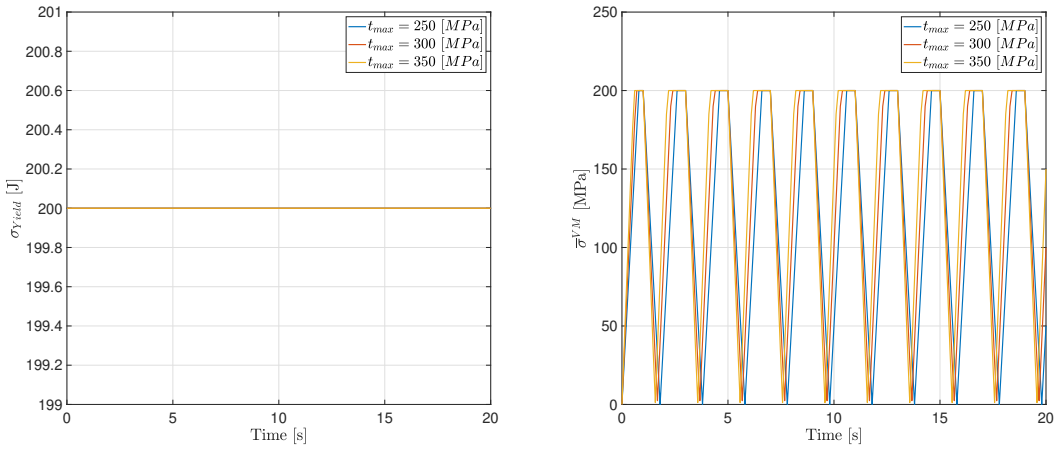

Figure 18: Evolution of the yield stress and the Von Mises yield stress with respect to the time in the case of a purely kinematic non-linear hardening law.

In the case of a purely kinematic non-linear hardening law, the yield surface is only subjected to a translation of its center. Indeed, its size remains constant since there are no isotropic effects. Therefore, the evolution of the backstress must look like a periodic function whose periodicity does not change over time. This observation is confirmed by the Fig. 19. It is important to notice that this behaviour is also expected regarding the equivalent backstress and one can see that this is indeed the case.

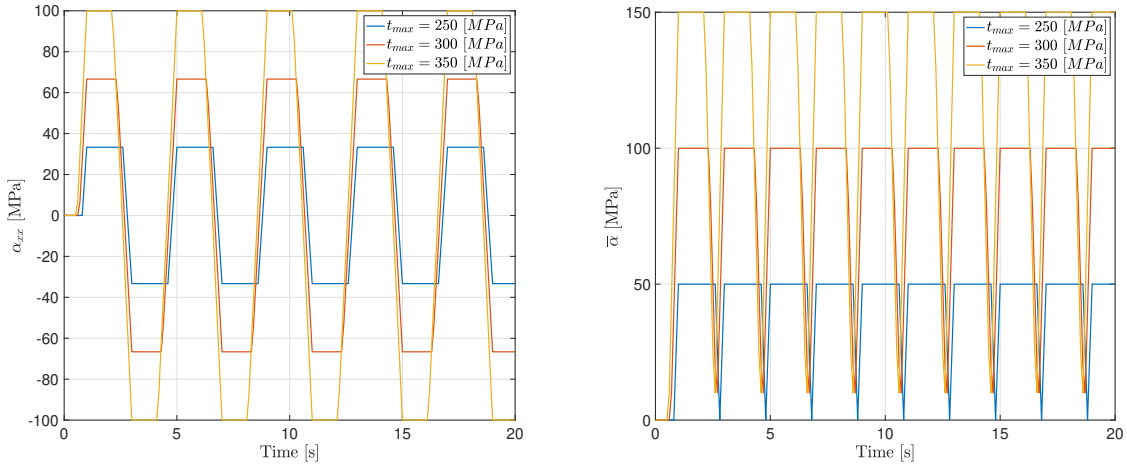

Figure 19: Evolution of the backstress and the equivalent back stress stress with respect to the time in the case of a purely kinematic non-linear hardening law.

Regarding the evolution of the effective plastic strain, as it can be observed in Fig. 20 that as the load increases, $\overline{\varepsilon}^p$ also does. From a physical point of view, this behaviour is expected. In addition to that, from the Fig. 19, one know that the maximum amplitude of the backstress increases as the load also increases. When the load almost reaches its maximum value, it implies that the backstress also almost reach its asymptotic value. The only way for the backstress to reach this value is by having the dynamic recovery effect full compensating the translation force. Thus, using the former observations made about the Eq. 2.35, one know that the intensity of the dynamic recovery force depends on the effective plastic strain since η_k is fixed. Therefore, this reasoning confirms the physical intuition regarding the behaviour of the evolution of $\overline{\varepsilon}^p$ with respect to the intensity of the load.

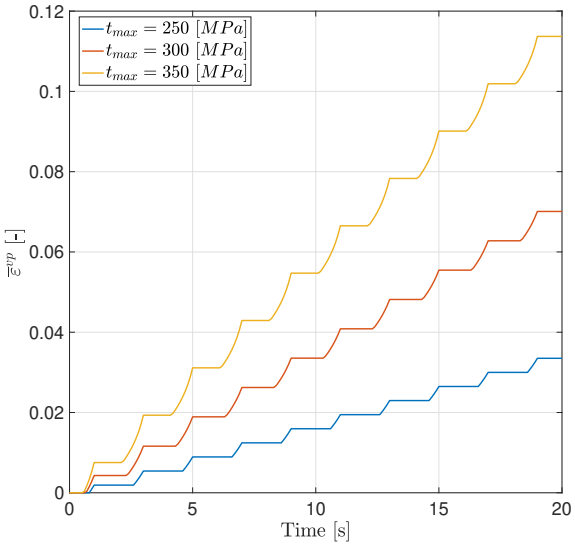

Figure 20: Evolution of the effective plastic strain with respect to the time in the case of a purely kinematic non-linear hardening law.

By contrast to elasticity, during a plastic process, energy is dissipated. In fact, around 10% of the energy is used to rearrange the atom whereas nearly 90% of the rest is lost due to heat dissipation.

Therefore, it is interesting to give a look at the energy dissipated during the plastic deformation process. In addition to that, one can compare the results with those coming from the linear kinematic case. The following figure is thus obtained.

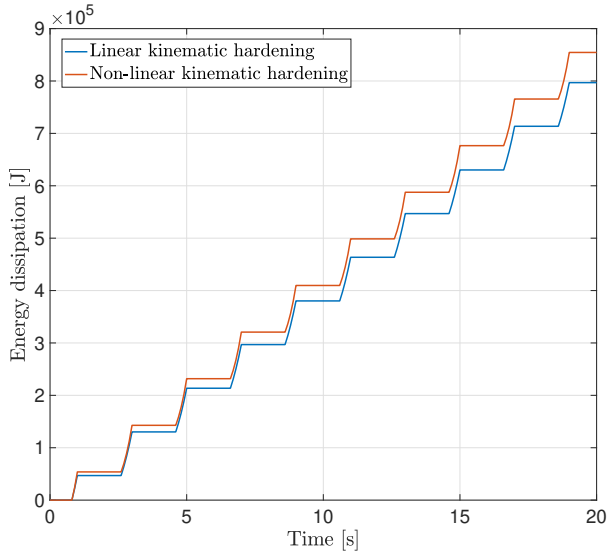

Figure 21: Evolution of the dissipated energy with respect to the time in the cases of a purely kinematic linear and non-linear hardening laws.

As it can be seen in Fig. 21, during the whole cycle, the energy dissipated by the non-linear kinematic hardening law is higher than for the linear kinematic. This phenomenon can be explained by first starting from the expression of the plastic energy dissipation which is expressed as:

$$\mathbb{D}^p = \bar{\sigma}\dot{\bar{\varepsilon}}^p = \bar{\sigma}\sqrt{\frac{2}{3}}\lambda. \tag{2.76}$$

Therefore, one observe that the plastic flow intensity λ plays an important role in the determination of the total dissipated energy. As a reminder, the value of the plastic multiplier in the case of a purely kinematic linear hardening law is defined as:

$$\lambda_{\text{Linear}} = \frac{N_{kl}D_{kl}}{1 + \frac{h}{3G}}. \tag{2.77}$$

In the non-linear case, the expression of λ can be derived from its general expression which is expressed as:

$$\lambda = \frac{\frac{\partial f}{\partial \sigma_{ij}}\mathbb{H}_{ijkl}D_{kl}}{\frac{\partial f}{\partial \sigma_{pq}}\mathbb{H}_{pqtu}N_{tu} - \frac{\partial f}{\partial \mathbf{q}^{(v)}} * r^{(v)}}. \tag{2.78}$$

This general equation can be simplified and adapted to the purely kinematic non-linear hardening law by using different assumptions. Indeed, as it was discussed previously, the derivative of the yield criterion with respect to the stress tensor for associated plasticity can be expressed as:

$$\frac{\partial f}{\partial \sigma_{ij}} = \frac{\partial f}{\partial s_{ij}} = \sqrt{\frac{3}{2}}N_{ij}. \tag{2.79}$$

In addition to that, the expression of Hooke's tensor can be developed as follows:

$$\mathbb{H}_{ijkl} = K\delta_{ij}\delta_{kl} + G(\delta_{ik}\delta_{jl} + \delta_{il}\delta_{kj} - \frac{2}{3}\delta_{ij}\delta_{kl}), \tag{2.80}$$

where K and G are respectively the bulk modulus and the shear modulus. If this tensor is multiplied by the unit tensor from Eq. 2.79, this gives

$$N_{ij}\mathbb{H}_{ijkl} = KN_{ii}\delta_{kl} + 2GN_{kl} - \frac{2G}{3}N_{ii}, \tag{2.81}$$

and using the fact that $\mathbf{N}$ is deviatoric, or in other words that $\mathtt{tr}\ \mathbf{N} = 0$, this expression can be finally written as:

$$N_{ij}\mathbb{H}_{ijkl} = 2GN_{kl}. \tag{2.82}$$

Finally, the internal variables α_{ij} and σ_y and their evolution laws are known such that the denominator can be developed easily. The following derivation is performed using a linear isotropic hardening of the yield stress in order to have a general expression which can be simplified to the considered case by posing $h = h_k$.

$$\begin{aligned}\frac{\partial f}{\partial \mathbf{q}^{(v)}} * r^{(v)} &= \frac{1}{\lambda}\left(\frac{\partial f}{\partial \alpha_{ij}}\dot{\alpha}_{ij} + \frac{\partial f}{\partial \sigma_y}\dot{\sigma}_y\right) \\ &= -\sqrt{\frac{3}{2}}N_{ij}\left(\frac{2}{3}h_k N_{ij} - \eta_k\sqrt{\frac{2}{3}}\alpha_{ij}\right) - \sqrt{\frac{2}{3}}h_i \\ &= -\sqrt{\frac{2}{3}}h + \eta_k N_{ij}\alpha_{ij},\end{aligned} \tag{2.83}$$

where $h = h_i + h_k$. The last term that can be developed is the first term of the denominator present in the Eq. 2.78. This can be achieved by using the results of Eq. 2.79 and 2.82, it leads to the following development:

$$\frac{\partial f}{\partial \sigma_{pq}}\mathbb{H}_{pqtu}N_{tu} = \sqrt{\frac{3}{2}}2GN_{tu}N_{tu} = \sqrt{\frac{3}{2}}2G. \tag{2.84}$$

Finally, using all the former equations, the numerator and the denominator of the plastic multiplier can be simplified into:

Numerator

$$\begin{aligned}(N) &= \frac{\partial f}{\partial \sigma_{ij}}\mathbb{H}_{ijkl}D_{kl} \\ &= \sqrt{\frac{3}{2}}2GN_{kl}D_{kl} \\ &= \sqrt{6}GN_{kl}D_{kl}.\end{aligned} \tag{2.85}$$

Denominator

$$\begin{aligned}(D) &= \frac{\partial f}{\partial \sigma_{pq}}\mathbb{H}_{pqtu}N_{tu} - \frac{\partial f}{\partial \mathbf{q}^{(v)}} * r^{(v)} \\ &= \sqrt{\frac{3}{2}}2G + \sqrt{\frac{2}{3}}h + \eta_k N_{ij}\alpha_{ij} \\ &= \sqrt{6}G + \sqrt{\frac{2}{3}}h + \eta_k N_{ij}\alpha_{ij}.\end{aligned} \tag{2.86}$$

By rearranging these terms, the final expression of the plastic multiplier λ in the case of a non-linear kinematic hardening law is therefore expressed as:

$$\lambda_{\text{Non-linear}} = \frac{N_{kl} D_{kl}}{1 + \frac{h}{3G} - \frac{\eta_k}{\sqrt{6}G} N_{ij}\alpha_{ij}}. \tag{2.87}$$

A simple comparison between this expression and the one given by Eq. 2.77 shows that the difference can be found in the denominator. Indeed, due to the non-linearity of the law, one can found that the dynamic recovery parameter has for effect to decrease the value of the denominator and thus increasing the value of the plastic multiplier. This observation explains why the evolution of the energy dissipated during the traction/compression process represented in Fig. 21 is higher in the case of the purely kinematic non-linear hardening law.

2.5 Non-linear kinematic hardening mixed with a linear isotropic hardening

From now on, the hardening law will be described by a non-linear kinematic hardening defined by Armstrong-Frederic's evolution law of the backstress tensor combined with a linear isotropic hardening of the yield stress. In this part also, the influence of the load will be studied for the same arbitrary fixed dynamic recovery parameter $\eta_k = 100$. First of all, the expression of the yield stress is given in this case by:

$$\sigma_y = \sigma_y^0 + h_i \bar{\varepsilon}^p. \tag{2.88}$$

Therefore, the evolution law for σ_y can easily be deduced from the former equation as follows:

$$\dot{\sigma}_y = h_i \dot{\bar{\varepsilon}}^p = h_i \sqrt{\frac{2}{3}} \lambda. \tag{2.89}$$

The asymptotic value of the yield stress can be inferred from Eq. 2.89. Indeed, this value is reached when $\dot{\sigma}_y = 0$ which is only possible when the effective plastic strain rate is also equal to zero, or in other words when the effective plastic strain does not evolve anymore. Due to the isotropic hardening, the value of the yield stress evolves over time. Therefore, once the yield stress reaches the maximum value of the loading, the material will stop undergoing plastic deformation. Thus, one can conclude that the asymptotic value in this case is :

$$\sigma_y^u = t_{max}. \tag{2.90}$$

This conclusion is in agreement with the numerical results showed on Fig. 22. However, if t_{max} is smaller than the initial yield stress, the asymptotic value is simply σ_y^0.

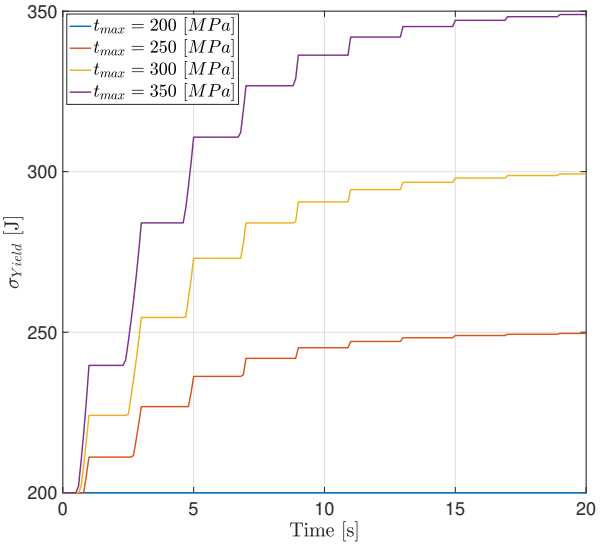

Figure 22: Evolution of the yield stress σ_y for different values t_{max} in the case of a mixed non-linear kinematic hardening law with a linear isotropic hardening law.

The non-linearity of the evolution can be explained using the Eq. 2.87, λ depends on α_{ij} which itself depends on time and the stress state. Therefore, if λ is time dependent and using Eq. 2.89, one can deduce that $\dot{\sigma}_y$ cannot be constant. Thus, σ_y does not evolve linearly with respect to time during the cycle. The term linear in the linear isotropic hardening law comes from the fact that the evolution of σ_y is linear in the effective plastic strain $\overline{\varepsilon}^p$. Regarding the equivalent Von Mises stress, its evolution is shown in Fig. 23. As it can be seen, there are two different behaviour observable depending on if t_{max} is higher than the initial yield stress $\sigma_y^0 = 200$ [MPa].

Indeed, if t_{max} is lower, the shape of the Von Mises stress remains the same during the cycle as plasticity is never reached and there is no hardening. However, if t_{max} is higher than the initial yield stress, an increase of the Von Mises stress is observed through the loading as the material hardens and the yield surface increases.

In addition to that, it is possible to observe that the consistency condition $f = 0$ is respected during plasticity as $\overline{\sigma}^{VM}$ is equal to σ_y during the hardening. One should also notice that $\overline{\sigma}^{VM}$ also tends to an asymptotic value equal to t_{max} due to its relation with the yield stress. Overall, the only influence of t_{max} is on the amplitude of the stress which tends in each case to the maximal value t_{max}.

In the case of the equivalent stress $\overline{\sigma}$, its evolution is represented on Fig. 24. Intuitively, its shape should remain constant during the loading as its expression does not depend on the backstress tensor. This intuition is in agreement with the numerical results since a constant periodic evolution of the stress can be observed. Once again, the only effect of t_{max} is to increase the maximum amplitude taken by $\overline{\sigma}$. Regarding the upper bound of $\overline{\sigma}$ in this case, its expression can be deduced simply by analogy with Eq. 2.73 as $\sigma_y^u = t_{\text{max}}$:

$$\overline{\sigma} \leq t_{\text{max}} + \frac{h_k}{\eta_k}. \tag{2.91}$$

From Eq 2.91, one can deduce that the upper bound does not have a sense as t_{max} can be increased independently of the material. As a consequence, there is no reason to express an asymptotic yield surface in this case.

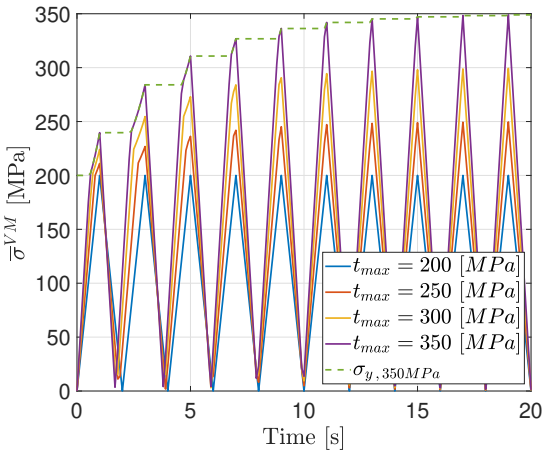

Figure 23: Evolution of the Von Mises equivalent stress for different t_{max} as well as the evolution of the yield stress for a mixed non-linear kinematic hardening with a linear isotropic hardening law.

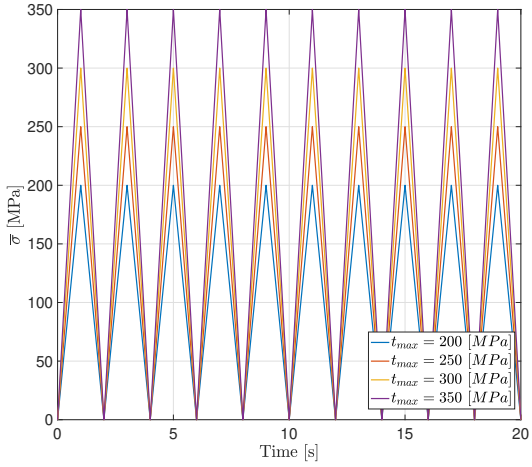

Figure 24: Evolution of the equivalent stress for different t_{max} for a mixed non-linear kinematic hardening with a linear isotropic hardening law.

Regarding the effective plastic strain, its evolution is represented on Fig. 25. As expected, if plasticity is not reached, $\overline{\varepsilon}^p$ remains equal to zero during the whole loading whereas if plasticity is reached, the effect of $t_{\max}$ is that $\overline{\varepsilon}^p$ increases faster and is higher at the end of the loading. In addition to that, it is also possible to observe that the time passed in plasticity becomes shorter throughout the cycles as the increments of $\overline{\varepsilon}^p$ become smaller and smaller. This is not surprising as the yield stress is evolving due to hardening. Therefore, plasticity is reached at a higher value of the yield stress at each cycle which reduces the duration of the plastic regime throughout the cycle. This asymptotic value of the plastic strain is reached faster for lower $t_{\max}$ as the stress level is lower.

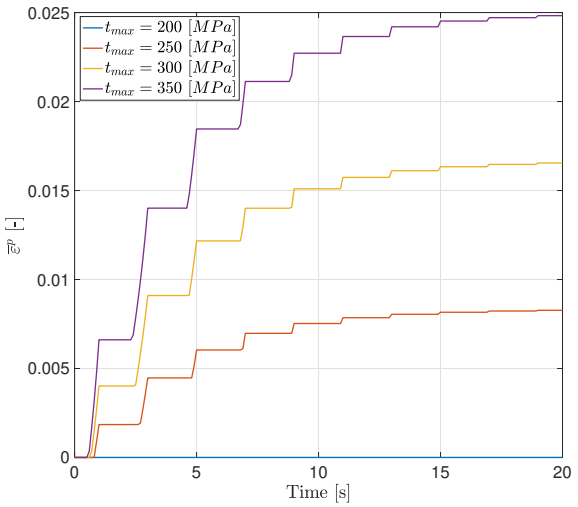

Figure 25: Evolution of the effective plastic strain for different $t_{\max}$ in the case of a mixed non-linear kinematic hardening law with a linear isotropic hardening law.

The last quantity to observe when isotropic hardening is taken into account is the equivalent backstress $\overline{\alpha}$, its evolution is shown in Fig. 26. In the first case with the load $t_{max} = 200[MPa]$ plasticity is not reached, the yield surface is not moving and thus $\overline{\alpha}$ is equal to 0 during the whole loading. However, on the other cases, the equivalent backstress converges to 0. Indeed, the yield stress is increasing until it reaches the maximal value $t_{\max}$. Hence, after this value has been reached, the cube does not enter anymore into the plastic domain which explains why $\overline{\alpha}$ converges towards 0. Moreover, $\overline{\alpha}$ has higher amplitudes for higher values of $t_{\max}$. This is also expected because for a higher level of stress, the surface will move more and thus the backstress has to be higher as the center of the surface is also moving further than its initial position.

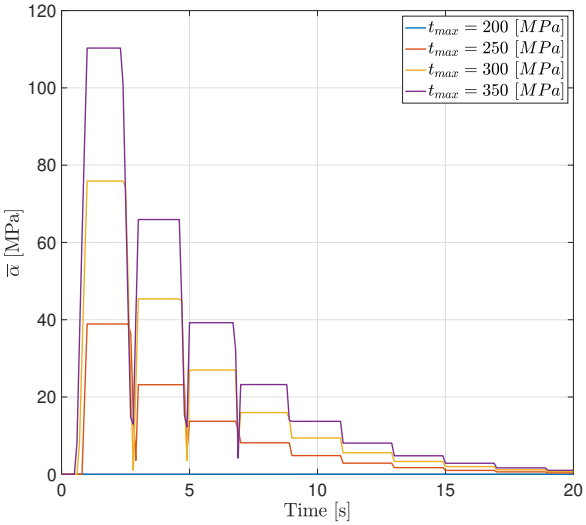

Figure 26: Evolution of the equivalent backstress for different $t_{\max}$ in the case of a mixed non-linear kinematic hardening law with a linear isotropic hardening law.

2.6 Non-linear kinematic hardening mixed with a non-linear isotropic hardening

In this last part, the hardening law will be described by a non-linear kinematic hardening defined by Armstrong-Frederic's evolution law of the backstress combined with a non-linear isotropic hardening of the yield stress describe by Voce's saturated law. Once again, the influence of the load will be studied for the same arbitrarily fixed dynamic recovery parameter $\eta_k = 100$.

First of all, the expression of the yield stress is given in this case by:

$$\sigma_y = \sigma_y^\infty - \left(\sigma_y^\infty - \sigma_y^0\right) \exp\left(-\frac{h_i \bar{\varepsilon}^p}{\sigma_y^\infty - \sigma_y^0}\right). \tag{2.92}$$

In comparison to Eq. 2.88, the law contains a decreasing exponential term which tends to saturate the evolution of the yield stress. This difference plays an important role since it affects the overall behaviour of every quantity that will be studied later on. From the former equation, it is possible to deduce the evolution law of the yield stress:

$$\begin{aligned}\dot{\sigma}_y &= \left(\sigma_y^\infty - \sigma_y^0\right) \cdot \frac{h_i \dot{\bar{\varepsilon}}^p}{\sigma_y^\infty - \sigma_y^0} \cdot \exp\left(-\frac{h_i \bar{\varepsilon}^p}{\sigma_y^\infty - \sigma_y^0}\right) \\ &= h_i \sqrt{\frac{2}{3}} \lambda \exp\left(-\frac{h_i \bar{\varepsilon}^p}{\sigma_y^\infty - \sigma_y^0}\right) \\ &= h_i \dot{\bar{\varepsilon}}^p \exp\left(-\frac{h_i \bar{\varepsilon}^p}{\sigma_y^\infty - \sigma_y^0}\right).\end{aligned} \tag{2.93}$$

The asymptotic value of the yield stress can be deduced from it. Indeed, using Eq. 2.93, one found that the evolution is equal to 0 if $\dot{\bar{\varepsilon}}^p = 0$, i.e. when the effective plastic strain remains constant or if the exponential term converges to 0, i.e $\bar{\varepsilon}^p = +\infty$. Therefore, the asymptotic values can be retrieved from Eq. 2.92 and they are:

$$\sigma_y^u = \begin{cases} \sigma_y^\infty = 300 \text{ [MPa]} & \textbf{if} \quad t_{max} \geq \sigma_y^\infty, \\ t_{max} & \textbf{if} \quad t_{max} < \sigma_y^\infty. \end{cases} \tag{2.94}$$

These values were expected as the saturated law was defined by the parameter σ_y^∞ which corresponds to the maximal value that can be reached by the subsequent yield stress. As it can be seen on Fig. 27, the conclusions of Eq. 2.94 are respected. Indeed, the yield stresses for $t_{max} = 200[MPa]$ and $t_{max} = 250[MPa]$ converges to these respected values whereas for the other 2 loads, they both converges as expected to the subsequent yield stress σ_y^∞. In the case of the Von Mises yield stress, the same behaviour as the one represented in Fig. 23 is expected. However, $\overline{\sigma}^{VM}$ must converge to σ_y^∞ for the two higher loads. The results are represented in Fig. 27.

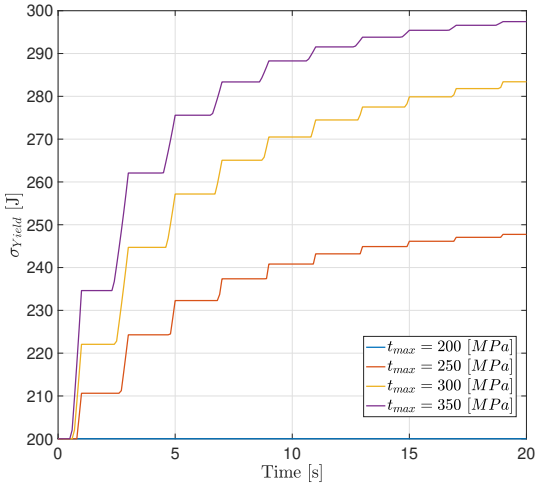

Figure 27: Evolution of the yield stress for different t_{max} in the case of a fully non-linear mixed kinematic and isotropic hardening law

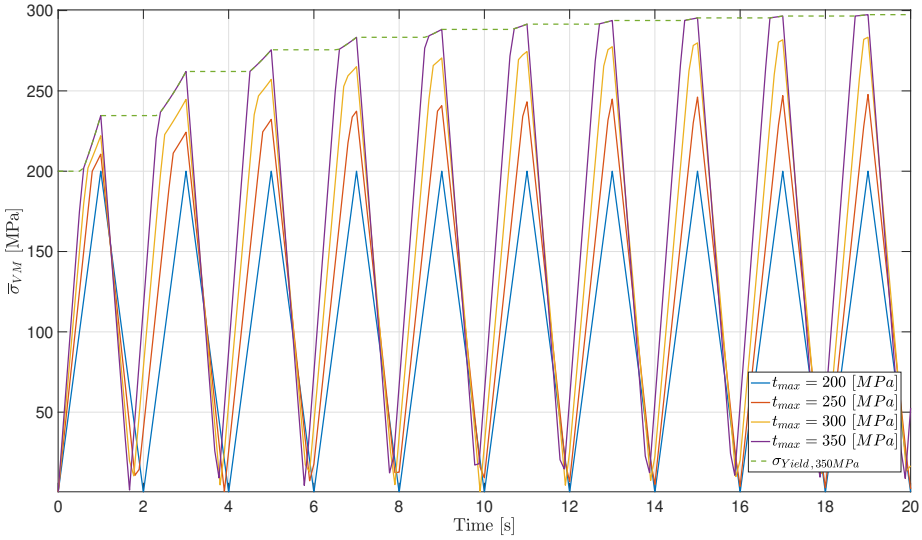

Figure 28: Evolution of the equivalent Von Mises stress for different $t_{\max}$ in the case of a fully non-linear mixed kinematic and isotropic hardening law

Regarding the equivalent stress and the effective plastic strain, the same observations that were made in the former section on Fig. 24 and 25 are also applicable here. Indeed, on Fig. 30, one can observe that the effective stress is also represented by a constant periodic function. Furthermore, since $\overline{\sigma}$ does not take into account the backstress, this explains why the maximum amplitude is equal to the maximum value taken by the load. In this case, an upper bound for the equivalent stress can be deduced from Eq. 2.73. Indeed, recalling that $\sigma_y^u = \sigma_y^\infty$ for the considered law, one can write:

$$\overline{\sigma} \leq \sigma_y^\infty + \frac{h_k}{\eta_k}. \tag{2.95}$$

Using this last equation, it is possible to define an asymptotic yield surface as in the purely kinematic case. By analogy with Eq. 2.74, the expression of this surface is given by:

$$f^u = \sqrt{3J_2} - \sigma_y^\infty - \frac{h_k}{\eta_k} \leq 0. \tag{2.96}$$

The asymptotic surface for a loading in traction is illustrated in Fig. 29. By opposition to the purely kinematic case, the size of the yield surface can change here and the size of the asymptotic surface correspond to the saturated stress level σ_y^∞ in this case. This correspond to the isotropic part of the hardening. Regarding, the kinematic part of the law, the discussion done for Fig. 17 still holds in this case. Indeed, the position of the asymptotic surface in traction corresponds to furthest position that can be reached during the loading in traction. In conclusion, during one loading cycle, the size of the yield surface and its position must be between the initial and the asymptotic surfaces.

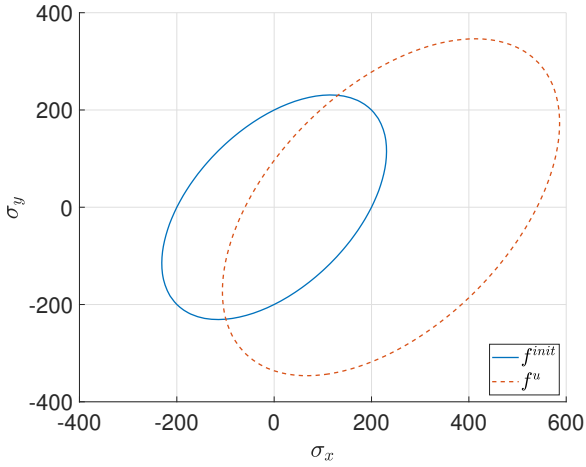

Figure 29: Asymptotic and initial yield surfaces for non-linear mixed hardening

Regarding the effective plastic strain represented in Fig. 31, its value increases as the value of $t_{\max}$ also increases. In addition to that, the time spent into the plastic domain also decreases throughout the whole cycle. However, one big difference between a fully mixed non-linear hardening law and the one from the former section resides in the evolution of the equivalent backstress tensor. Indeed, by contrast to the result obtained in Fig. 26, in this situation $\overline{\alpha}$ does not necessarily converges to 0.

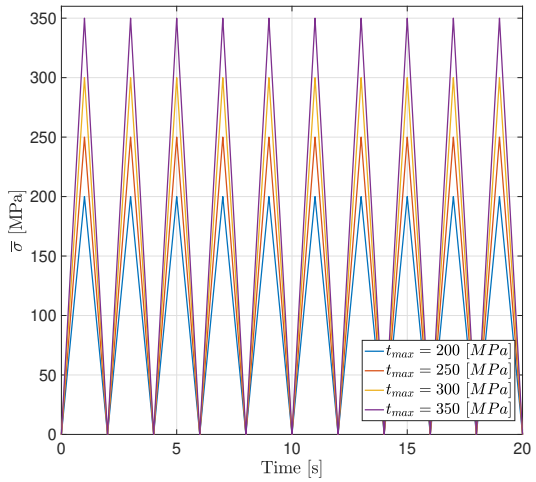

Figure 30: Evolution of the effective stress for different $t_{\max}$ in the case of a fully non-linear mixed kinematic and isotropic hardening law

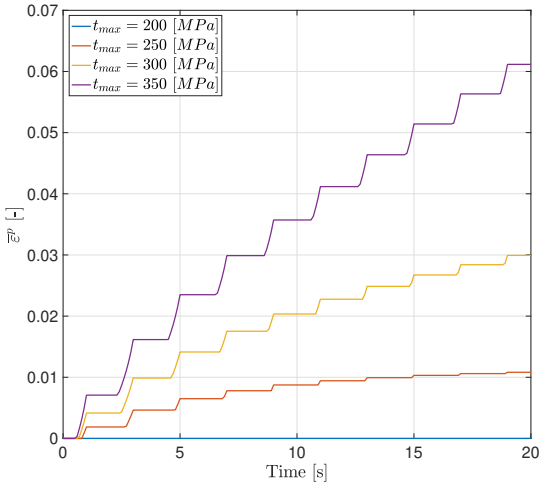

Figure 31: Evolution of the effective plastic strain for different $t_{\max}$ in the case of a fully non-linear mixed kinematic and isotropic hardening law

Indeed, as it can be seen on the Fig. 32, the equivalent backstress seems to converge only for certain values of the load. This can be explained using Voce's saturated law. In the case of the load $t_{\max} = 250$ [MPa], this value is lower than σ_y^∞ therefore at some point, the yield stress is equal tho $t_{\max}$ such that the cube does not reach plasticity anymore. This is why $\overline{\alpha} = 0$ in that case. However, if the load is greater than σ_y^∞, the isotropic behaviour of the cube will be saturated. In other words, only the kinematic effect of the hardening remains. If the number of cycle tends to infinity, the equivalent backstress should reach a state of periodicity with constant amplitude such as the one described in the case of purely kinematic hardening.

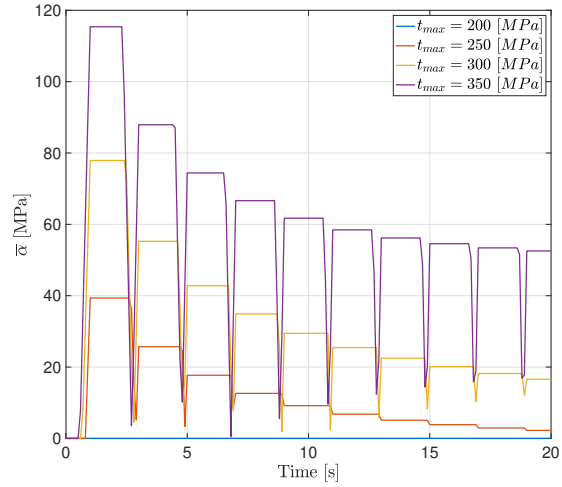

Figure 32: Evolution of the equivalent backstress for different $t_{\max}$ in the case of a fully non-linear mixed kinematic and isotropic hardening law

Part 3 - Study of elasto-viscoplastic behavior

This third part aims to study the elasto-viscoplastic behavior of the cube with an isotropic and a mixed hardening model. By contrast to the previous cases, the behaviour of the cube is now rate-dependent. Therefore, the period of the loading will impact the results. Based on Melan's hypothesis and Drucker's postulate, the flow rule can be expressed as follows:

$$\mathbf{D}^{vp} = \lambda \mathbf{N}. \tag{3.97}$$

The main differences with the elasto-plastic model is the definition of the so-called flow intensity λ. The elasto-viscoplastic model is based on *Perzyna*'s model and therefore the flow intensity can be written as:

$$\lambda = \sqrt{\frac{3}{2}} \left\langle \frac{\bar{\sigma} - \sigma_y}{\eta \left(\bar{\varepsilon}^{vp}\right)^n} \right\rangle^{\frac{1}{m}} \quad \begin{cases} = 0 \text{ in elasticity ,} \\ > 0 \text{ in plasticity.} \end{cases} \tag{3.98}$$

where,

- $\frac{1}{n}$ being a hardening exponent;
- $\frac{1}{m}$ being a viscosity exponent;
- $\langle x \rangle = \frac{1}{2}(x + |x|)$ are the *Mc Auley* brackets.
- η is the viscosity parameter. By performing a simple dimensional analysis, it is possible to deduce the unit of this parameter:

$$[\eta] = [\sigma]/[\lambda] \quad \text{where} \quad [\lambda] = [\mathcal{D}^{vp}] = \frac{1}{\text{s}}, \tag{3.99}$$

thus,

$$[\eta] = \text{Pa . s} = \frac{\text{kg}}{\text{m s}}. \tag{3.100}$$

Then, concerning the hardening criterion, the extended consistency condition is defined as follows:

$$\bar{f} = \bar{\sigma} - \sigma_y - \eta(\bar{\varepsilon^{vp}})^n(\dot{\bar{\varepsilon}}^{vp})^m = 0. \tag{3.101}$$

In this study, the parameters n and m are imposed to:

$$m = 1 \quad \text{and} \quad n = 0. \tag{3.102}$$

Therefore, the Perzyna's law and the extended consistency condition become:

$$\lambda = \sqrt{\frac{3}{2}} \left\langle \frac{\bar{\sigma}^{VM} - \sigma_{\text{y}}}{\eta} \right\rangle, \tag{3.103}$$

$$\bar{f} = \bar{\sigma}^{VM} - \sigma_y - \eta\dot{\bar{\varepsilon}}^{vp} = 0. \tag{3.104}$$

The main difference with the classical consistency condition is that in the extended case, the stress state can be located outside of the yield surface whereas it is strictly prohibited in the non-viscous case. The radial distance between the state and the yield surface is by definition the overstress expressed as:

$$d = \bar{\sigma} - \sigma_y = \eta \dot{\bar{\varepsilon}}^{vp}. \tag{3.105}$$

It can be represented in Haigh Westergaard's space as illustrated in Fig. 33.

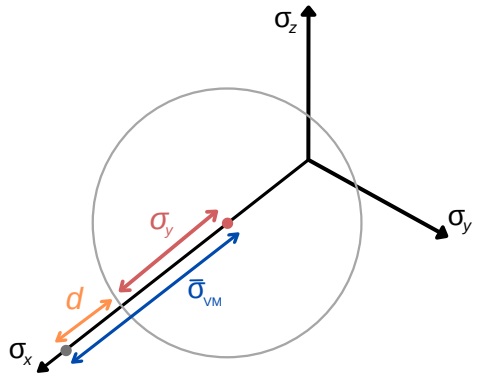

Figure 33: Over-stress representation in the Haigh Westergaard's space.

3.1 Relevant variables

The different relevant variables and the hardening law that are presented in the part 1 can be re-expressed for the elasto-visco plastic model as:

$$\dot{\bar{\varepsilon}}^{vp} = \sqrt{\frac{2}{3}\boldsymbol{D}^{vp} : \boldsymbol{D}^{vp}} = \sqrt{\frac{2}{3}}\lambda = \left\langle \frac{\bar{\sigma}^{VM} - \sigma_y}{\eta} \right\rangle, \tag{3.106}$$

$$\dot{\sigma}_y = h_i \dot{\bar{\varepsilon}}^{vp} = h_i \left\langle \frac{\bar{\sigma}^{VM} - \sigma_y}{\eta} \right\rangle, \tag{3.107}$$

$$\dot{\boldsymbol{\alpha}} = \frac{2}{3} h_k \lambda \boldsymbol{N} = \sqrt{\frac{2}{3}} h_k \boldsymbol{N} \left\langle \frac{\bar{\sigma}^{VM} - \sigma_y}{\eta} \right\rangle. \tag{3.108}$$

Similarly to the inviscid case, all these evolution laws in the case of an elastic process are equal to zero. Indeed, if the state of stress is smaller than the current yield stress, the flow intensity is zero thanks to the *Mc Auley* brackets properties.

3.2 Influence of the viscosity parameters and determination on the limit cases

First, it seems relevant to study the effect of the viscosity by varying the value of η between 0 and 10^7 [MPa.s]. Based on the simulations in Fig. 34a and 34b, it seems important to highlight the fact that the viscosity parameter does not delay the first entrance in plasticity. To understand that, the consistency condition can be expressed in the elastic field where $\dot{\bar{\varepsilon}}^{vp} = 0$ such that :

$$\bar{f} = f = \bar{\sigma}^{VM} - \sigma_y \tag{3.109}$$

Thus, the classical Von Mises criterion is recovered and η has no influence on the first entrance in plasticity. However, the amplitude of the first plastic strain increment is strongly influenced by this parameter. Indeed, the larger η, the smaller the amplitude is as shown in Fig. 34a and 34b. Then, one can notice that for the largest parameter, i.e. $\eta = 10^7$[MPa.s], the cube will tend to behave like an elastic material in such a way that the equivalent plastic strain tends to 0 as expected. The other limit case is obtained by imposing $\eta = 0$ [MPa.s]. In such condition, there is no viscous effect and the results are the same as those obtained in the first part of this project.

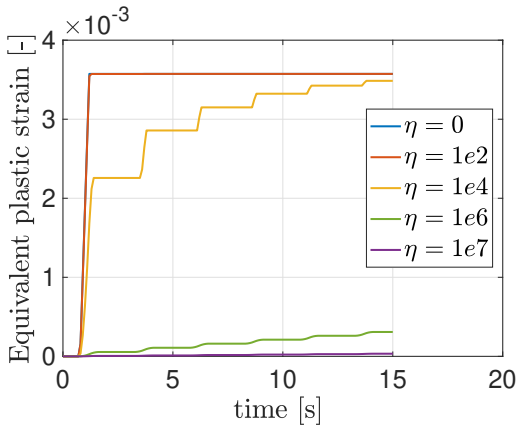

(a) The equivalent plastic strain for an isotropic hardening model.

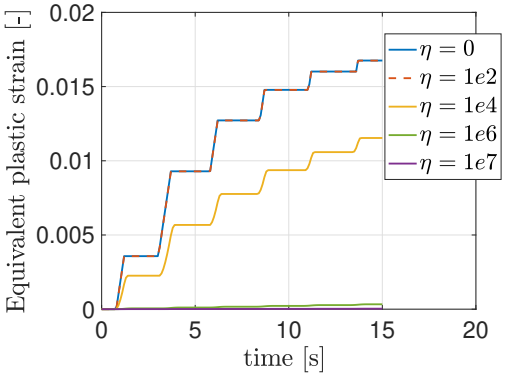

(b) The equivalent plastic strain for a mixed hardening model.

Figure 34: The equivalent plastic strain for an elasto-viscoplastic model with different value of the viscosity parameters.

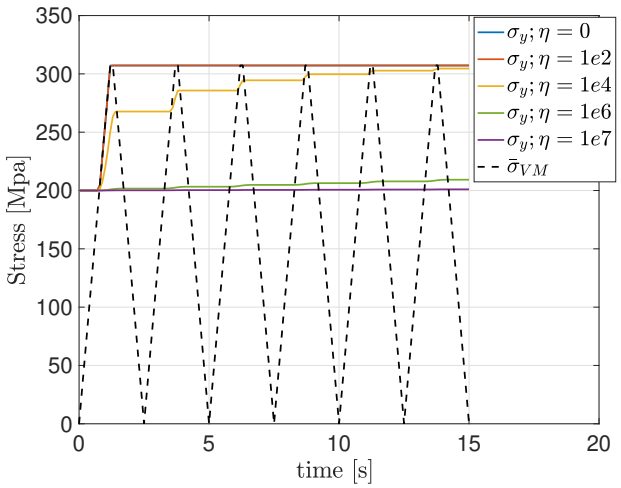

(a) The current yield stress for isotropic hardening model.

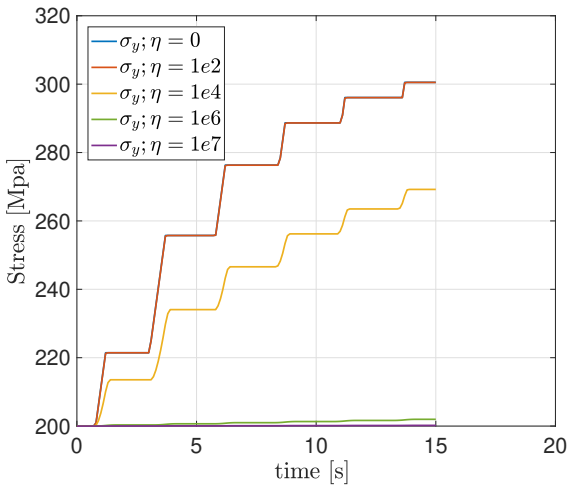

(b) The current yield stress for mixed hardening model.

Figure 35: The current yield stress for an elasto-viscoplastic model with different value of the viscosity parameters.

Then, as expected from the previous analysis, Fig. 34a, 34b, 35a and 35b reveal that viscosity allows to attenuate the rise of the plastic strain and of the yield stress. Physically, the plasticity corresponds to the spread of the dislocations allowing the plastic slip. Therefore, the viscosity characterizes the resistance to the dislocation glide in the material such that a high viscosity leads to a low equivalent plastic deformation. It is thus possible to understand that if the viscosity tends to the infinity, there is no plastic process since the dislocations have no mobility. Conversely, if there is no viscosity, the plasticity is time insensitive given that the dislocations can spread instantaneously through the material. To make the link with the yield stress, it is useful to remind that the hardening corresponds to the accumulation of dislocations around defects in the material. Thus, if the plasticity is limited by the viscosity, it is the same about the yield stress rise.

Finally, Fig. 36 illustrates the evolution of the overstress for an isotropic model. It can be observed that the maximum overstress decreases over the time. This observation can be explained by the fact that the yield surface grows during the hardening and get closer to the maximum stress state over the cycles.

Moreover, it is important to notice that the larger η, the lower the decrease of the maximum overstress over the cycles. This is due to the fact that a larger η implies a lower hardening and thus a lower growth of the yield surface.

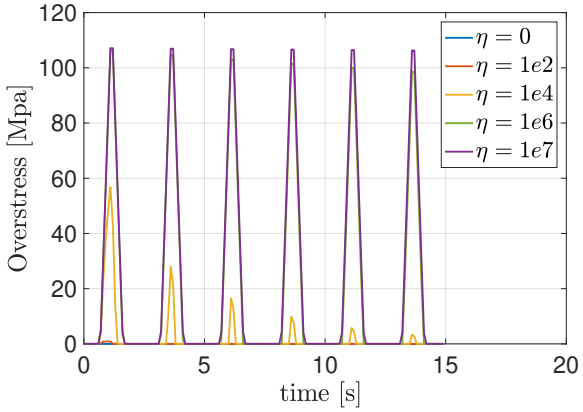

Figure 36: The overstress for an isotropic model submitted to several loading/unloading cycles.

3.3 Analysis of the different loading

3.3.1 Loading 1

The purpose of this section is to understand the elasto-viscoplastic strain evolution if the applied force is kept at its maximum value t_{max} for a infinitely long time as shown in Fig. 37. First, the mathematical expression of the plastic strain can be established for an elasto-viscoplastic behaviour without hardening and for an isotropic hardening. Considering only the plateau, it comes $t(t) = t_{\text{max}}$ [MPa] over $t \in [t_s; \infty[$ where t_s is the beginning time of the plateau. The plane stress state allows to writes $\sigma_x = t_{\text{max}}$.

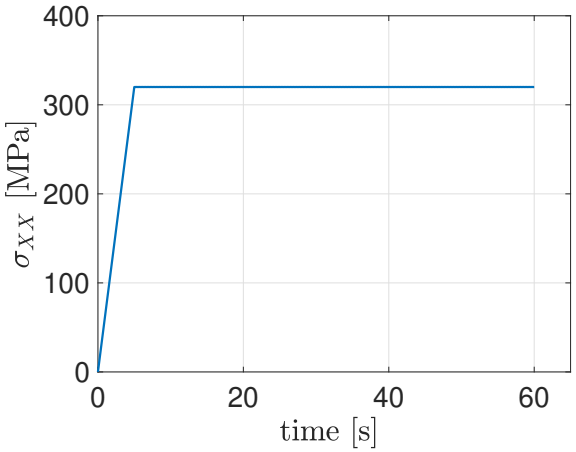

Figure 37: Representation of the loading.

Given that both considered cases present a zero backstress, $\bar{\sigma} = \sigma_x = t_{\text{max}}$ in such a way the yield stress and the equivalent plastic strain rate are expressed as:

$$\dot{\bar{\varepsilon}}^{vp} = \left\langle \frac{t_{\text{max}} - \sigma_y}{\eta} \right\rangle, \tag{3.110}$$

$$\dot{\sigma}_y = h_i \dot{\bar{\varepsilon}}^{vp} = h_i \left\langle \frac{t_{\text{max}} - \sigma_y}{\eta} \right\rangle. \tag{3.111}$$

Perfectly plastic

The first considered case is the perfectly plastic model such that $\dot{\sigma}_y = 0$ and therefore, $\sigma_y(t) = \sigma_y^0$. Given the plastic range such that $t_{\max} > \sigma_y$ and the initial condition $\bar{\varepsilon}^{vp}(t = t_s) = \bar{\varepsilon}_s^{vp}$, it comes:

$$\bar{\varepsilon}^{vp}(t) = \bar{\varepsilon}_s^{vp} + \left(\frac{t_{\max} - \sigma_y^0}{\eta}\right) \cdot t. \tag{3.112}$$

Since $t_{\max} \geq \sigma_y^0$ for all $t \in [t_s; \infty[$, the asymptotic limit is:

$$\bar{\varepsilon}^{vp}(+\infty) \to +\infty. \tag{3.113}$$

Given the plastic range such that $t_{\max} > \sigma_y$ and the initial condition $\bar{\varepsilon}^{vp}(t = t_s) = \bar{\varepsilon}_s^{vp}$, it comes:

$$\bar{\varepsilon}^{vp}(t) = \bar{\varepsilon}_s^{vp} + \left(\frac{t_{\max} - \sigma_y^0}{\eta}\right) \cdot t. \tag{3.114}$$

Since $t_{\max} \geq \sigma_y^0$ for all $t \in [t_s; \infty[$, the asymptotic limit is:

$$\bar{\varepsilon}^{vp}(+\infty) \to +\infty. \tag{3.115}$$

Thus, the equivalent plastic strain will tend to infinity at a rate inversely proportional to the viscosity parameter η. Hence, η allows to decrease the plastic strain rate. Indeed, the first limit case $\eta = 0$ leads to an infinitely large increase of the plastic strain while the other limit $\eta \to \infty$ enables to avoid it during the plateau. Finally, these theoretical developments and observations are in accordance with the results given by *Metafor* shown in Fig. 38.

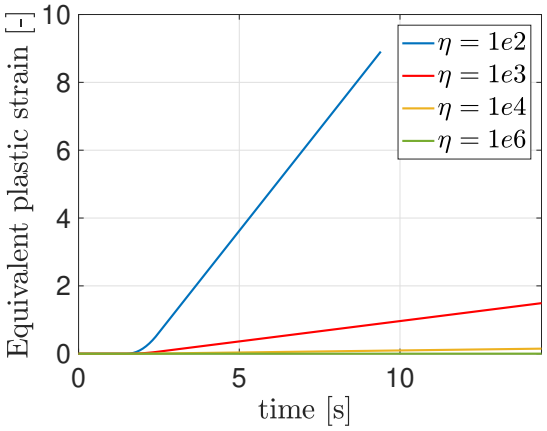

Figure 38: The equivalent plastic strain for a perfectly plastic model.

Isotropic hardening

The second case is the isotropic hardening. By integrating the relation 3.111 with the condition $\sigma_y(t_s) = \sigma_{y,s}$, it comes:

$$\sigma_y(t) = (\sigma_{y,s} - t_{\max}) \exp\left[\frac{h_i}{\eta}(t_s - t)\right] + t_{\max}. \tag{3.116}$$

This expression allows to deduce the asymptotic expression of the yield stress such that $\sigma_y(\infty) = t_{\max}$ for any η. This theoretical result is illustrated in Fig. 39b with simulations using $t_s = 5$ [s]. Then, after substituting σ_y in the Eq. 3.110, $\dot{\bar{\varepsilon}}^{vp}$ is expressed as:

$$\dot{\bar{\varepsilon}}^{vp} = \frac{(t_{\max} - \sigma_{y,s})}{\eta} \exp\left[\frac{h_i}{\eta}(t_s - t)\right] > 0. \tag{3.117}$$

Then, the integration with the condition $\bar{\varepsilon}^{vp}(t = t_s) = \bar{\varepsilon}^{vp}_s$ leads to:

$$\bar{\varepsilon}^{vp}(t) = \bar{\varepsilon}^{vp}_s + \frac{(t_{\max} - \sigma_{y,s})}{h_i}\left[1 - \exp\left(\frac{h_i}{\eta}(t_s - t)\right)\right]. \tag{3.118}$$

This relation is valid when $t_{\max} \geq \sigma_y(t)$, which is verified for all $t \in [t_s; \infty[$. It is thus possible to deduce the asymptotic value of $\bar{\varepsilon}^{vp}$ when the time tends to infinity as:

$$\bar{\varepsilon}^{vp}(+\infty) = \bar{\varepsilon}^{vp}_s + \frac{(t_{\max} - \sigma_{y,s})}{h_i}. \tag{3.119}$$

This asymptotic value in function of η for a given t_s can be computed using the values of $\bar{\varepsilon}^{vp}_s$ and $\sigma_{y,s}$ obtained from the simulations. Numerically, with $t_s = 5$ [s], the simulations shown in Fig. 39a allow to get:

$$\bar{\varepsilon}^{vp}(+\infty) = 0.4 \ [\%] \quad \forall \eta. \tag{3.120}$$

Given that the case $\eta = 0$ is time independent, it is thus possible to claim that the asymptotic value is not only independent of the parameter η but also of the loading time t_s. However, it is important to keep in mind that the speed of convergence is directly influenced by the parameter η such that a larger η leads to a slower convergence as seen in Fig. 39a. Indeed, by analyzing the limit cases, if $\eta = 0$, the asymptotic value is directly reached while for $\eta = \infty$, it takes an infinite time, which corresponds to an elastic system.

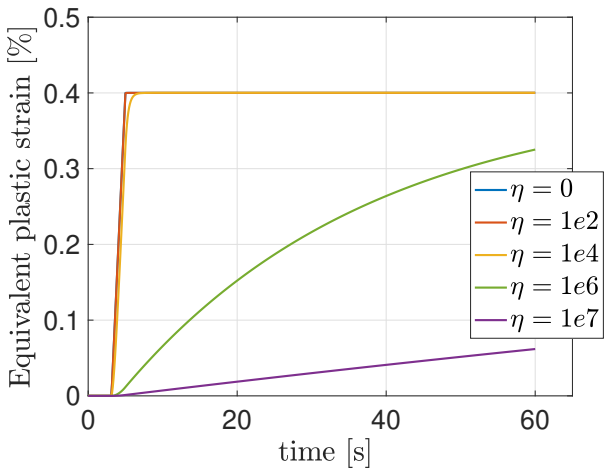

(a) The equivalent plastic strain for an isotropic hardening model.

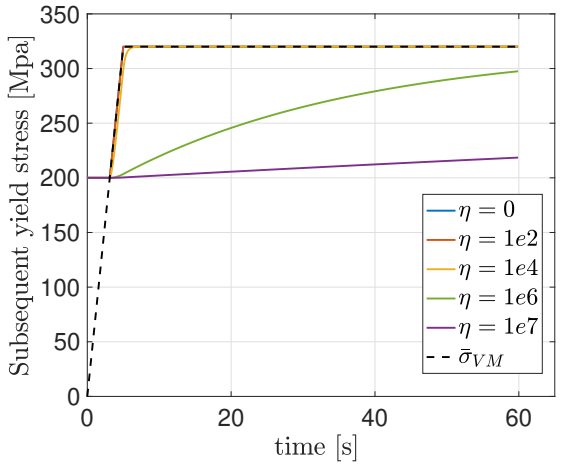

(b) The subsequent yield stress for an isotropic model.

Figure 39: The equivalent plastic strain and subsequent yield stress for an isotropic hardening for $t_s = 5$ [s].

Mixed hardening

In the case of a mixed model in plane stress, the equivalent stress is the same as the isotropic case such that $\bar{\sigma} = t_{max}$. Thus, the deviatoric tensor can be expressed as:

$$\mathbf{s} = t_{max} \cdot \text{diag}(2/3, -1/3, -1/3). \tag{3.121}$$

Concerning the backstress tensor, basing on the results from the simulations, this quantity can be written as follows:

$$\boldsymbol{\alpha} = \alpha \cdot \text{diag}(1, -1/2, -1/2). \tag{3.122}$$

Thus, the equivalent backstress is such that:

$$\bar{\alpha} = \frac{3}{2}\alpha. \tag{3.123}$$

It is now possible to determine the expression of the Von Mises stress using the Eq. 3.121 and 3.122:

$$\bar{\sigma}^{VM} = \bar{\sigma} - \bar{\alpha} = t_{\text{max}} - \bar{\alpha}. \tag{3.124}$$

This expression enables to rewrite the rate of the yield stress and the x-component α of the backstress tensor during the hardening:

$$\begin{cases} \dot{\sigma}_y = \frac{h_i}{\eta}\left[\bar{\sigma}^{VM} - \sigma_y\right] \\ \dot{\alpha} = \sqrt{\frac{2}{3}}\frac{h_k}{\eta} N_x \left[\bar{\sigma}^{VM} - \sigma_y\right] \end{cases} \Rightarrow \quad \begin{cases} \dot{\sigma}_y = \frac{h_i}{\eta}\left[t_{\text{max}} - \bar{\alpha} - \sigma_y\right] \\ \dot{\bar{\alpha}} = \frac{h_k}{\eta}\left[t_{\text{max}} - \bar{\alpha} - \sigma_y\right] \end{cases} \tag{3.125}$$

with,

$$N_x = \frac{(s_x - \alpha_x)}{\sqrt{(\mathbf{s} - \boldsymbol{\alpha}) : (\mathbf{s} - \boldsymbol{\alpha})}} = \sqrt{\frac{2}{3}}. \tag{3.126}$$

That allows to deduce the ratio between both rates:

$$\dot{\sigma}_y = \frac{\theta}{(1-\theta)}\dot{\bar{\alpha}} = \frac{1}{4}.\dot{\bar{\alpha}} \tag{3.127}$$

Integrating both Eq. 3.125 with the initial conditions $\sigma_y(t = t_s) = \sigma_{y,s}$ and $\bar{\alpha}(t = t_s) = \bar{\alpha}_s$ gives:

$$\begin{cases} \sigma_y = (1-\theta)\sigma_{y,s} - \theta\left(\bar{\alpha}_s - t_{\text{max}}\right) + \theta\left(\bar{\alpha}_s + \sigma_{y,s} - t_{\text{max}}\right)\exp\left[\frac{h}{\eta}\left(t_s - t\right)\right], \\ \bar{\alpha} = \theta\bar{\alpha}_s + (1-\theta)\left[t_{\text{max}} - \sigma_{y,s}\right] + (\theta - 1)\left[t_{\text{max}} - \bar{\alpha}_s - \sigma_{y,s}\right]\exp\left[\frac{h}{\eta}\left(t_s - t\right)\right]. \end{cases} \tag{3.128}$$

Knowing the expression of σ_y and $\bar{\alpha}$, the equivalent plastic strain rate during the hardening can be expressed as:

$$\dot{\bar{\varepsilon}}^{vp} = \frac{1}{\eta} \cdot \left[\left[t_{\text{max}} - \bar{\alpha}_s - \sigma_{y,s}\right]\exp\left[\frac{h}{\eta}\left(t_s - t\right)\right]\right]. \tag{3.129}$$

Based on the simulations for $\eta = 10^6$ [MPa.s] and $t_s = 5$ [s], it is possible to claim $\left[\bar{\varepsilon}^{vp}\right]_{mixed} = \left[\bar{\varepsilon}^{vp}\right]_{iso}$ since:

$$\left[t_{\text{max}} - \bar{\alpha}_s - \sigma_{y,s}\right]_{mixed} = \left[t_{\text{max}} - \sigma_{y,s}\right]_{iso} = 203.48 \text{ [MPa]} \quad \text{and} \quad [h]_{mixed} = [h_i]_{iso}$$

$$\Rightarrow \left[\dot{\bar{\varepsilon}}^{vp}\right]_{mixed} = \left[\dot{\bar{\varepsilon}}^{vp}\right]_{iso}.$$

with the initial conditions

$$[\bar{\varepsilon}_s^{vp}]_{mixed} = [\bar{\varepsilon}_s^{vp}]_{iso} = 1.16 \cdot 10^{-2}[\%].$$

Thus, the expression obtained for the isotropic case is the same as in the mixed case. To understand qualitatively this result, it seems relevant to focus on the evolution of the equivalent backstress $\bar{\alpha}$, the yield stress σ_y and the Von Mises stress for a given η as shown in Fig. 40a. On one hand, $\bar{\alpha}$ increases in the flow direction until reaching a plateau. Since the equivalent stress $\bar{\sigma} = t_{\text{max}}$ is constant, the rise of $\bar{\alpha}$ implies a decrease of $\bar{\sigma}^{VM}$. One the other hand, the yield stress increases much slower than the isotropic case. That can be explained by the fact that $h_{i,\text{iso}} = h$ for the isotropic case while $h_{i,\text{mixed}} = 0.2h$ such that the yield stress rate is 5 times weaker in the mixed case.

Finally, the decrease of $\bar{\sigma}^{VM}$ is balanced by the slower increase of σ_y in such a way that the overstress $d = \bar{\sigma}^{VM} - \sigma_y$, illustrated in Fig. 40b, is the same for both cases and thus the plastic strain evolution is identical. Knowing the expression of σ_y in the isotropic case during the plateau, it is possible to deduce the expression of the overstress which is expressed as:

$$d = (t_{\text{max}} - \sigma_{y,s}) \exp\left[\frac{h_i}{\eta}(t_s - t)\right]. \tag{3.130}$$

Therefore, the limit $d(\infty) = 0$ such that the stress state tends to return to the yield surface.

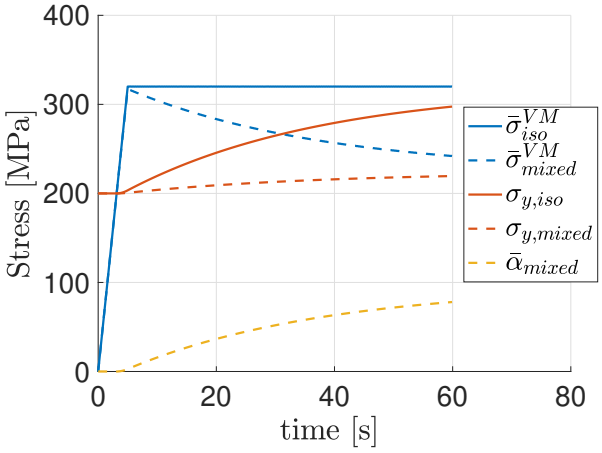

(a) Von Mises stress $\bar{\sigma}^{VM}$, yield stress σ_y and backstress $\bar{\alpha}$.

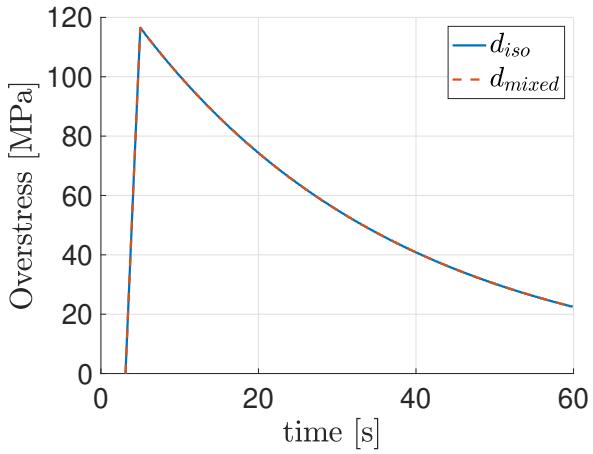

(b) Overstress.

Figure 40: Comparison between the mixed and isotropic model for a viscosity parameter $\eta = 10^6$ [MPa s].

Loading time influence

To extend this study, the effect of the loading time on the equivalent plastic strain can be analyzed. To do so, the viscosity parameter is fixed at 10^4 [MPa.s] and the loading is imposed at 0.25, 1, 2 and 3 [s]. Note that only the isotropic model can be considered given that, as observed above, the evolution of the plastic strain and of the overstress are the same for both models.

As shown in Fig. 41, the maximum overstress $d_{\max}$ reached at $t_{\max}$ is larger for a shorter loading time. Then, once the maximum value is reached, the overstress decreases until reaching a zero value for all cases. That can be geometrically interpreted as the return of the stress state on the yield surface in Haigh Westergaard's space. The higher $d_{\max}$ and the shorter loading, the longer this return is. Physically, during the plastic process, the shorter loading time leads to more irreversibilities such that the dislocations need more time to recover a stable state. Therefore, the overstress allows to characterize the duration to recover a stable case due to the dislocations glide through the material.

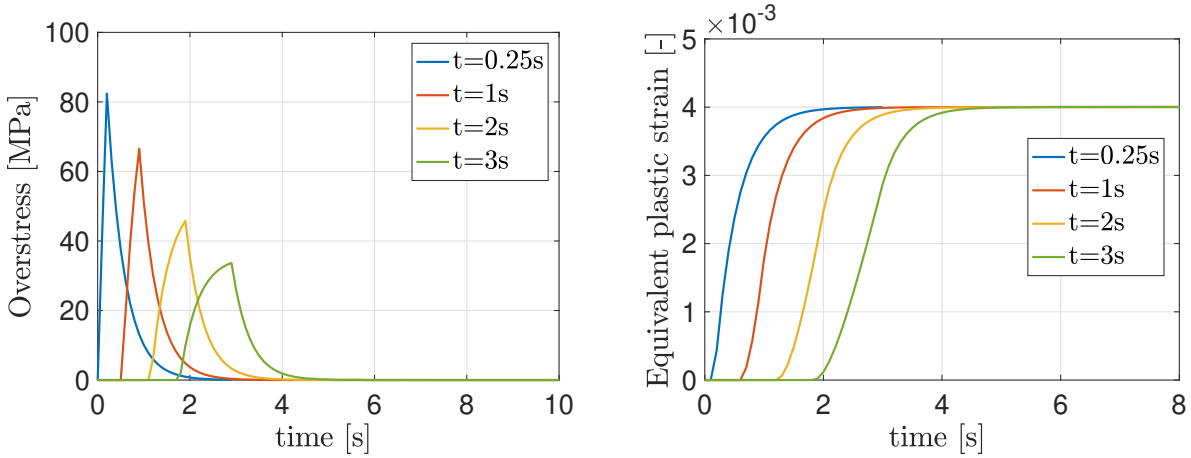

Figure 41: Influence of the loading speed over the overstress and the equivalent plastic strain.

3.3.2 Loading 2

The second considered loading is the initial one at which steps are added as it is shown in Fig. 42. In this case, the viscosity parameter is imposed at 10^6 [MPa.s]. Considering the isotropic and mixed hardening respectively shown in Fig. 43a and 43b, one should note that each plateau at $t_{\max}$ and $-t_{\max}$ induces a rise of the yield stress. This observation allows to illustrate the viscous effect given that for the elasto-plasticity, the plateaus do not imply hardening.

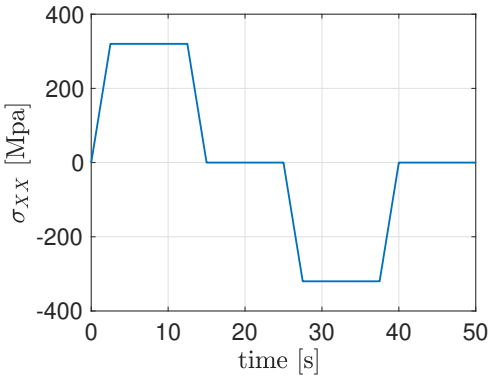

Figure 42: Loading with steps

Concerning the isotropic model in Fig. 43a, the equivalent Von Mises stress $\bar{\sigma}^{VM}$ remains constant during the different plateaus of the loading and is equal to $t_{\max}$. This is due to the absence of backstress such that the yield surface does not move in the stress space. Consequently, $\bar{\sigma}^{VM}$ takes the same value whether $\sigma_x = t_{\max}$ or $\sigma_x = -t_{\max}$.

Regarding the mixed hardening in Fig. 43b, the introduction of a viscosity implies a significant change for the evolution of the equivalent backstress. Indeed, there is not a continuous decrease of this parameter as observed for the non-viscous case but the plateau value is larger after a traction

than after a compression. Therefore, the Bauschinger effect is stronger in traction. Moreover, for a sufficiently long time, the plateau tends, in both cases, to the same value and the Bauschinger effect tends to be the same in both loading senses.

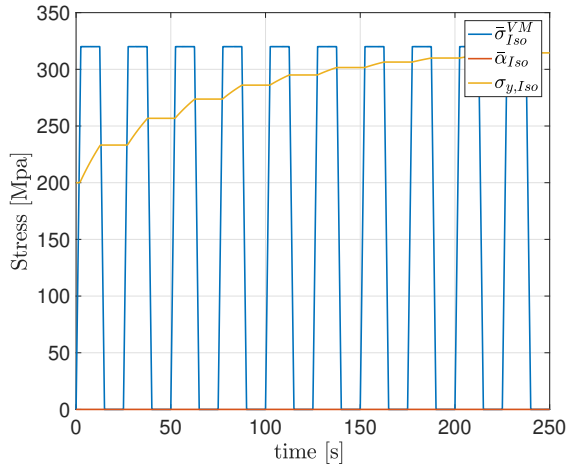

(a) The subsequent yield stress, the Von Mises stress for an isotropic model for a loading with steps and a value of $\eta = 10^6$ [MPa.s].

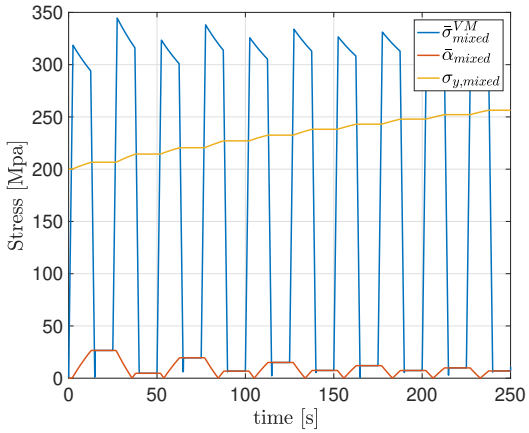

(b) The subsequent yield stress, the Von Mises stress and the equivalent backstress for an mixed model for a loading with steps and a value of $\eta = 10^6$ [MPa.s].

Figure 43

The evolution of $\bar{\alpha}$ allows to understand the maximum value reached by $\bar{\sigma}^{VM}$ once the loading is maximum. As illustrated in Fig. 44, once $\sigma_x = t_{\text{max}}$ for the first loading, the center is translated to the stress state in such way that $\bar{\sigma}^{VM}$ decreases during the plateau. Then, once $\sigma_x = -t_{\text{max}}$, the Von Mises stress reaches a larger peak than the past one due to the shift caused by the previous traction. One more time, the center gets closer to the current stress state and the Von Mises stress decreases. Since the equivalent backstress is higher after a traction than a compression, it seems thus logical that the maximum value of $\bar{\sigma}^{VM}$ is higher in compression.

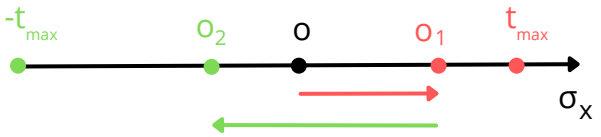

Figure 44: Representation of the first loading for the mixed hardening. The point O, O_1 and O_2 respectively stand for the position of the center of the yield surface along σ_x at $t = 0$ [MPa] (virgin state), $t = t_{\text{max}}$ [MPa] and $t = -t_{\text{max}}$ [MPa].

Part 4 - Sensitivity study of numerical parameters

In this last section, the influence of the numerical parameter on the simulation results for each type of hardening models previously discussed with a viscous parameters of $\eta = 10^4$ [MPa.s] will be studied. Indeed, it is important to verify that the results are valid from a numerical and physical point of view. In order to so, one can observe the influence of the:

- Loading speed
- Spatial discretization
- Temporal discretization

on the evolution of the internal work, external work and the equivalent plastic strain. In fact, the complexity difference between a 2D and 3D plastic deformation problem is enormous. Therefore, if one wishes to solve such a problem, it is needed to use a finite difference method in order to solve it numerically. In most cases, the method used is the principal of virtual work which states that in equilibrium the virtual work of the forces applied to a system is zero. In other words, the work done by the internal forces of the structure must be fully compensated by the work done by the external forces. The expression of these works is given by:

$$W_{\text{Int}} = \int_0^{t_f} \left(\vec{F}^{\,\text{Int}}(t) \cdot \dot{\vec{q}}(t) \right) dt \quad \text{and} \quad W_{\text{Ext}} = \int_0^{t_f} \left(\vec{F}^{\,\text{Ext}}(t) \cdot \dot{\vec{q}}(t) \right) dt, \tag{4.131}$$

with,

- $\vec{F}^{\,\text{Int}}(t)$: the internal forces;
- $\vec{F}^{\,\text{Ext}}(t)$: the applied forces;
- $\dot{\vec{q}}(t)$: the structural nodal velocity vector.

By contrast, in elasticity the search of a solution is done by looking for an equilibrium position which can be achieved using the principle of minimum of TPE where the total potential energy is expressed as:

$$TPE = U - P, \tag{4.132}$$

with,

- U : the elastic (internal) potential energy, which correspond to the internal work;
- P : the work done by the constant applied force, which correspond to the external work.

However, in the case of plastic problems, this principle is not valid anymore due to the non-linear relationship between stress and strain. Thus, the validity of the results cannot be assessed using the minimum TPE method. In addition to that, the method of virtual work does not make too much sense in the case of elasticity. Indeed, in this case, the internal parameters do not evolve during the plastic deformation. Therefore, $\dot{\vec{q}}(t)$ is equal to 0 all along. Nevertheless, in plasticity, an equilibrium position can be found using the principle of virtual work, where the inertia forces are neglected. From a physical point of view, the equilibrium configuration states that:

$$\underbrace{\vec{F}(t)^{OOB}}_{\text{out of balance forces}} = \vec{F}^{\,\text{Int}}(t) - \vec{F}^{\,\text{Ext}}(t) = 0. \tag{4.133}$$

However, from a numerical point of view, the out of balance forces will never be equal to 0 due to the approximations used by the method and the numerical computation errors. Thus, in the case of Metafor, the software assumes that the equilibrium position is found if

$$\vec{F}(t)^{OOB} < \epsilon, \tag{4.134}$$

where ϵ correspond to a tolerance usually set around 10^{-4}.

4.1 Influence of the loading speed

In order to observe the influence of the loading speed, the period T_{cycle} of the loading/compressing cycle is modified. Indeed, if the period decreases, the loading rate increases and vice versa. In addition to that, the other parameters of the simulation will be set to the following constant values:

- The number of cycles is equal to 3 [-];
- The number of elements is fixed to 1.
- The applied force is set to $t_{max} = 320$ [MPa];
- The temporal time step is fixed at 0.1[s];

Elasto-plastic model with linear isotropic hardening

It is important to remember that elasto-plastic models are rate independent, therefore the loading rate must not influenced the different values taken by the works. Since the works possesses the same order of magnitude, only the external work will be used for the different discussions. As it can be seen on figure (45), the value of W_{Ext} oscillates for the 10 first T_{cycle} tested. However, passing this threshold, its value seems to become more stable and even converge at the end. These observations are in contradiction with the fact that the model is supposed to be rate independent. This contradiction with theory come from numerical problems. Indeed, from a physical point on view, it becomes harder to impose the value of the maximum traction, t_{max}, if the period becomes smaller.

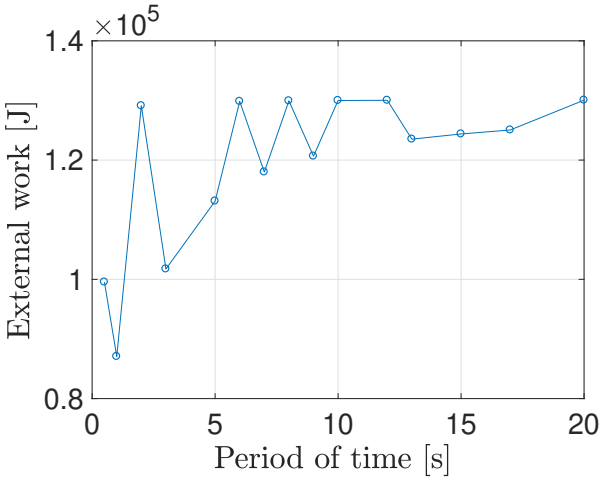

Figure 45: Final value of W_{Ext} for different loading rates using an elasto-plastic model with linear isotropic hardening.

In the limit case where the period tends towards 0, the value of t_{max} would have to be instantaneously imposed on the cube which is physically impossible. This leads to some contradiction with theory, thus it is necessary to impose a relatively large period of time in order to prevent this phenomena from happening. In addition to that, it is also interesting to observe the evolution of the equivalent plastic strain represented on Fig. 46. These results reveal that the first increment of the equivalent plastic strain becomes the same for a period of cycle larger than 10 seconds, which is in agreement with the results of Fig. 45.

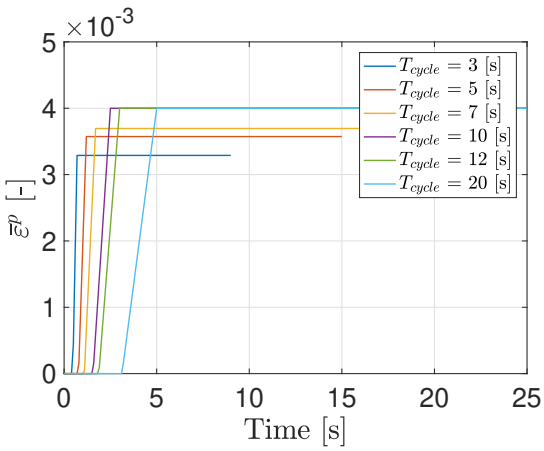

Figure 46: First increment of the equivalent plastic strain for different period of one cycle using an elasto-plastic model with linear isotropic hardening.

Elasto-plastic with non-linear kinematic hardening

As for the previous model, the theory predicts that the results should be rate independent. However, as it can be seen on Fig. 47 and 48, this is still not the case since both figures show the same phenomena seen previously. Once again, the value of the external work hardly vary for small period of cycle and converges when the period becomes larger than 7 seconds. In addition to that, the equivalent plastic strain represented on Fig. 47 shows that the value of the first increment of the equivalent plastic strain become constant once a period larger than 7 seconds is reached.

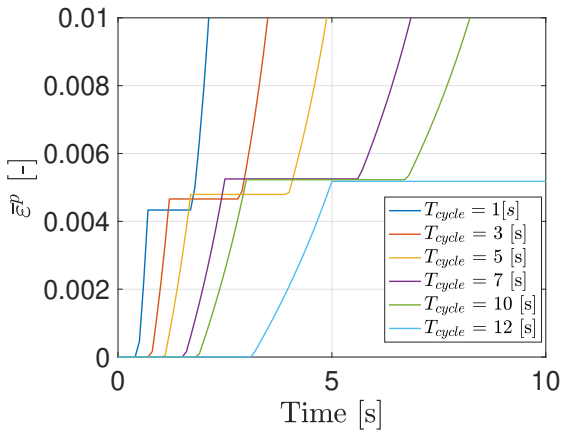

Figure 47: First increment of the equivalent plastic strain for different period of one cycle using an elasto-plastic with non-linear kinematic hardening.

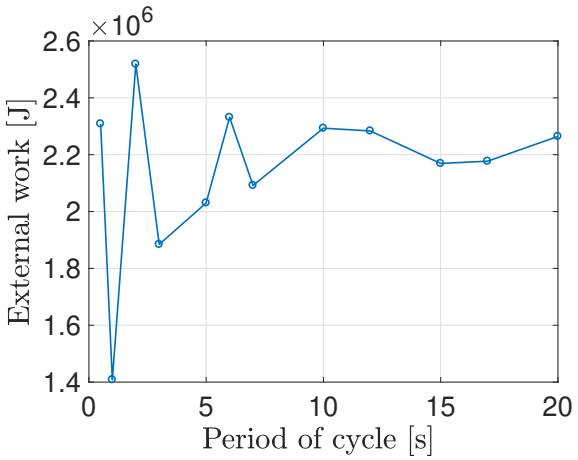

Figure 48: Final value of W_{Ext} for different loading rates using an elasto-plastic with non-linear kinematic hardening.

Elasto-viscoplastic with isotropic linear hardening

This last model is supposed to be the only one theoretically time dependent. Therefore, it is expected that the loading rate is going to influence the different quantity observed. As it can be seen, Fig. 50 shows that the evolution of the final value of W_{Ext} is always increasing much smoother than previously. Once again, the external work converges for period larger than 10 seconds. Even if this model is rate dependent, a too short period of time will lead the numerical solver to make errors. In the case of the equivalent strain, the Fig. 49 shows that it increases with the period of time but does not converge even for period larger than 10 seconds due to the rate dependency of the model.

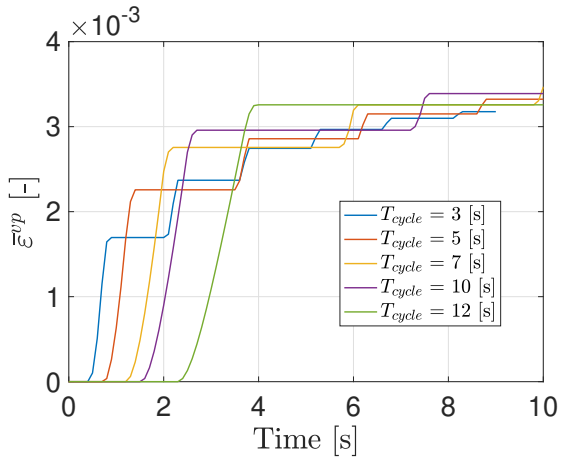

Figure 49: First increment of the equivalent plastic strain for different period of one cycle using an elasto-viscoplastic with isotropic linear hardening.

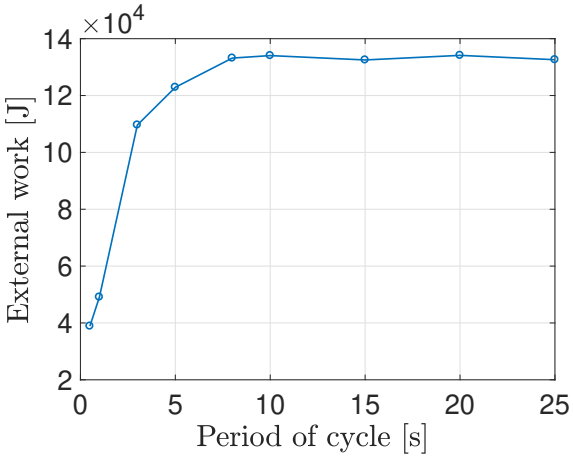

Figure 50: Final value of W_{Ext} for different loading rates using an elasto-viscoplastic with isotropic linear hardening.

4.2 Influence of spatial discretization

In this part of the analysis, the impact of the spatial discretization is studied by observing this time the final value taken by W_{Ext} and W_{Int}. During the simulations, the following parameters are kept constant for the three different models:

- The time step $\Delta_t = 0.1$[s];
- The number of cycles $N = 5$[-];
- The applied forces $t_{max} = 320$ [MPa];
- The period of each cycles, $T_{cycles} = 4$[s];

It is important to take into account that there is no interest in studying the equivalent plastic strain. Indeed, its value is computed at specific points and thus its value is independent of the mesh used on the cube. The results obtained for the different hardening laws are represented on Fig. 51, 52 and 53.

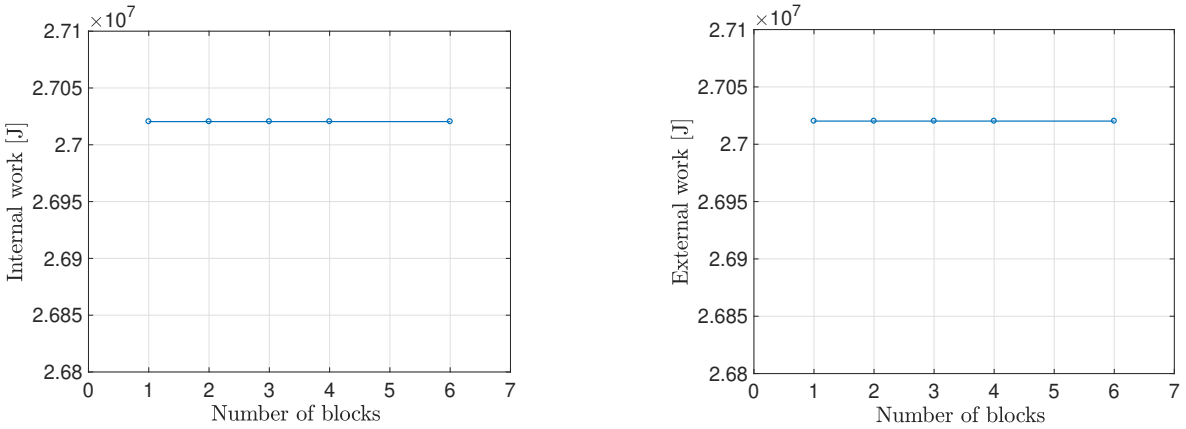

Figure 51: Final value taken by W_{Int} and W_{Ext} on the whole period in function of the number of elements by side in the case of an elasto-plastic with linear isotropic hardening.

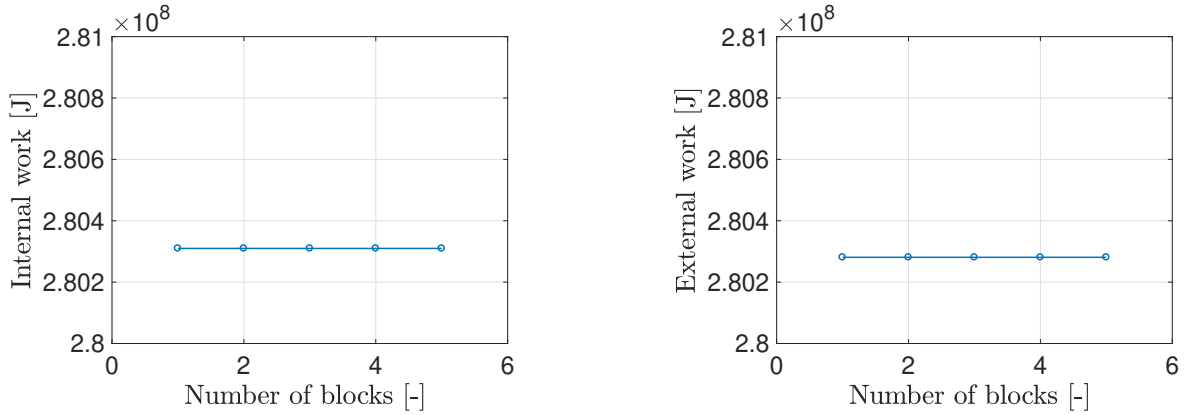

Figure 52: Final value taken by W_{Int} and W_{Ext} on the whole period in function of the number of elements by side in the case of an elasto-plastic with non-linear kinematic hardening.

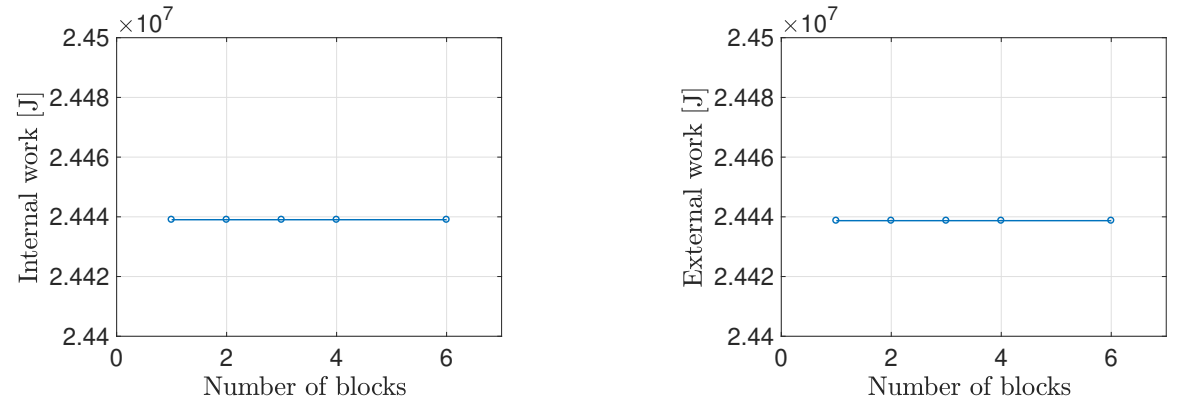

Figure 53: Final value taken by W_{Int} and W_{Ext} on the whole period in function of the number of elements by side in the case of an elasto-viscoplastic with isotropic hardening.

A first observation is that, in each case, the two works have a constant value whatever the number of elements. In addition to that, one know that the numerical solution has found solution for the cube at equilibrium since W_{Int} and W_{Ext} have almost exactly the same value. In conclusion, the spatial discretization has no influence whatsoever on the numerical results. Therefore, in order to reduce the computational cost, a spatial discretization of 1 element is considered to be the best option.

4.3 Influence of the temporal discretization

Finally, the influence of the temporal discretization is discussed by varying the time step. In this case, the goal is to find a sufficiently large time step in order to reduce as much as possible the computational cost while having a small enough value to capture all the different features of the loading such as the maximum and minimum values taken by it. During the simulations, the parameters are set to these different values:

- The number of cycles: $N = 3$ [-].
- The loading cycle $T_{cycle} = 10$ [s];
- The applied for $t_{max} = 320$ [MPa];
- Temporal discretization of 1 element per side;

Elasto-plastic model with linear isotropic hardening

It is possible to observe on Fig. 54 that imposing a maximum time step $\Delta_t \leq 0.1[s]$ leads to a constant work. Indeed, if the time step is higher, the numerical solution does not take into account the eccentricities of the loading which leads to a rather poor accuracy. The same discussion can be made regarding Fig. 55. Therefore, in order to maximise the accuracy of the results and minimise the computational cost, the optimal time step is in this case $\Delta_t = 0.1$[s].

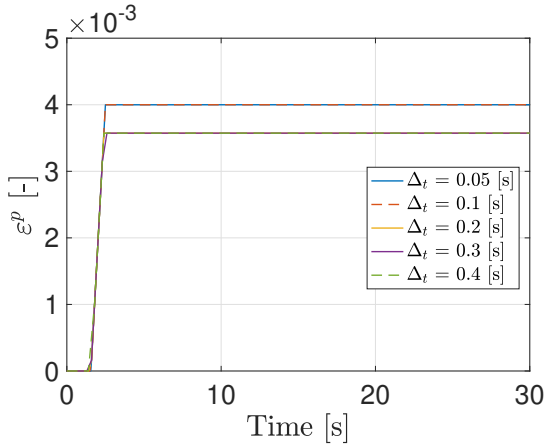

Figure 54: First increment of the equivalent plastic strain for different time steps using an elasto-plastic model with linear isotropic hardening.

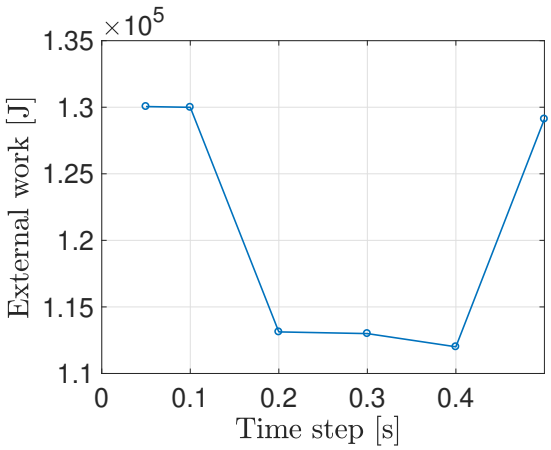

Figure 55: Final value of W_{Ext} for different time steps using an elasto-plastic model with linear isotropic hardening.

Elasto-plastic with non-linear kinematic hardening

The Fig. 56 and 57 lead to the same observations as for the former hardening law. Indeed, as the time step increases a larger, the results from one simulation to another increases more and more leading to an accuracy worst than the previous one. By looking at Fig. 57, it is possible to conclude that the most precise solution is for $\Delta_t = 0.05$ [s] but it comes with the price of increasing the computational cost. Thus, as a compromised, one can chose for optimal time step $\Delta_t = 0.1$ [s].

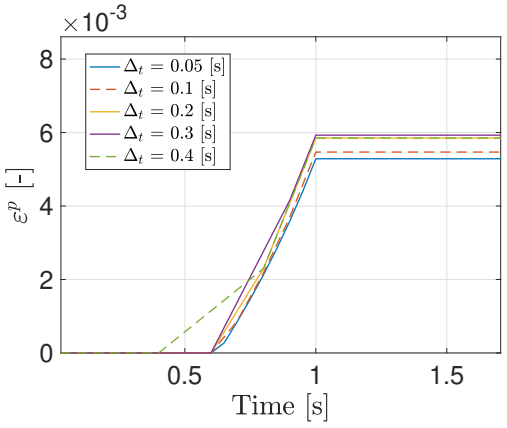

Figure 56: First increment of the equivalent plastic strain for different time steps using an elasto-plastic model non-linear kinematic hardening.

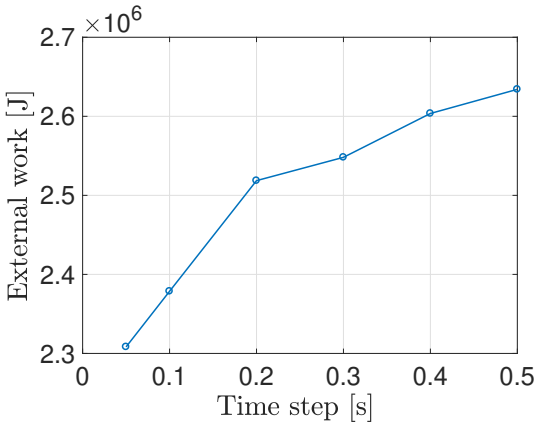

Figure 57: Final value of W_{Ext} for different time steps using an elasto-plastic model with non-linear isotropic hardening.

Elasto-viscoplastic with isotropic linear hardening

The results obtained from the numerical simulations are represented on the Fig. 58 and 59. The same discussion can be made regarding the optimal value of Δ_t.

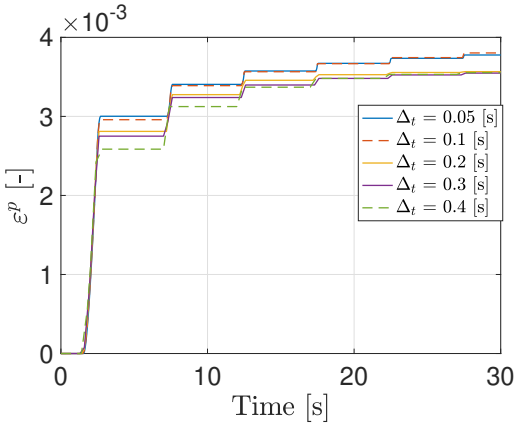

Figure 58: First increment of the equivalent plastic strain for different time steps using an elasto-viscoplastic with isotropic linear hardening.

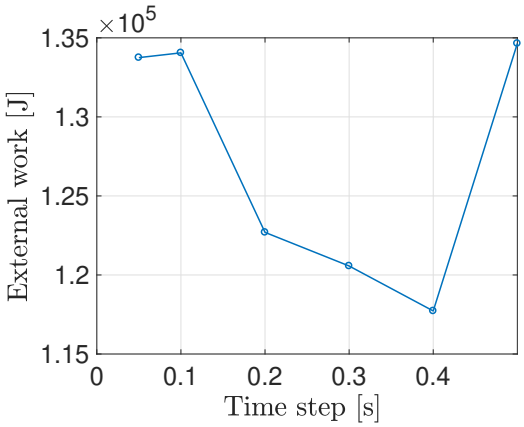

Figure 59: Final value of W_{Ext} for different time steps using an elasto-viscoplastic with isotropic linear hardening.

In conclusion, from the different analysis, one can conclude that the best numerical parameters are:

Numerical parameters	Period of cycle [s]	Number of elements [–]	Maximum time step [s]
Elasto-plastic linear hardening	10	1	0.1
Elasto-plastic non-linear hardening	7	1	0.1
Elasto-viscoplastic	10	1	0.1

Table 3: The best suited numerical parameters for different types of hardening laws.

As it can be observe on Table 3, the parameters are roughly of the same order of magnitude. Therefore, by setting the period of cycle to 10 s, one could run any simulation knowing that the best compromised between accuracy and computation time is almost reached in each case using this following combination of parameters.

Conclusion

This project allowed to study the behaviour of a cube submitted to a uni-axial loading. The goal was to understand how the cube behaves during a plastic process. The system was assumed to be elasto-plastic and different hardening model have been studied in plane stress and plane strain state. Those are the perfectly plastic, isotropic, kinematic and mixed linear hardening models.

The first part allowed to understand the different linear hardening models and especially their geometric representation in the stress space. The isotropic model is represented by a fixed yield surface growing during the hardening. Conversely, the kinematic case corresponds to a yield surface that translates as a rigid body. The mixed case is a combination of the two previous ones. It is represented by a moving surface with increasing dimensions. Considering the limit cases, for the isotropic and mixed models, the surfaces tend to a limit in such a way that the plastic strain rate and the dissipation rate end up by vanishing. Therefore, there is no more hardening and the stress state remains inside the hyper-volume defined by the yield surface. This limit case allowed to illustrate the shakedown effect during which the limit state remains on the same elastic stress-strain curve. By contrast, the yield surface of the kinematic model alternates between two extreme surfaces which are anti-symmetric with respect to the center of the stress space. Thus, the plastic process remains until the end of the loading and this leads to infinite equivalent plastic strain and plastic dissipation. Finally, it has been observed that the plane strain state leads to a residual stress when the loading takes a zero value. Regarding its asymptotic limit value, it tends to zero for the considered mixed model ($\theta = 0.2$) but to non zero values for the isotropic and kinematic hardening laws.

The second part of the project focused on the non-linear effects described by Armstrong-Frederick's evolution law of the backstress tensor. Indeed, this law introduces a new factor called the dynamic recovery parameter into the problem whose purpose is to simulate better the Bauschinger effect. In addition to that, the effect of the dynamic recovery was studied on all the other physical quantities such as the dissipation of energy, the stresses, the strains and so on. The differences with the linear case have been highlighted through the analysis of relevant quantities such as the plastic dissipation.

The third part allowed to understand the effects of the viscosity parameter η. Physically, this one stands for the resistance to the propagation of dislocations through the material. Those dislocations correspond to the plastic process. The higher η, the higher the resistance and therefore, the lower the equivalent plastic strain. Thus, the hardening in a viscous system is weaker given that it is linked to the accumulation of dislocations around the defects. This physical interpretation allows to understand the limit cases induced by η. On one hand, if $\eta = 0$, the dislocations can instantaneously moves and the model is time insensitive as seen in the first part. On the other hand, if $\eta \to \infty$, the dislocations cannot spread and the system is totally elastic. Then, the main difference with the non-viscous case is that the viscous system can harden under a constant loading. If the loading time is infinite, the yield stress and the equivalent plastic strain both tend to asymptotic limits which are the same for the isotropic and mixed hardening models. This process is characterized by the overstress which traduced the radial distance between the yield surface and the stress state. For a sufficiently long time, it ends up by vanishing as the plastic strain rate, which translates the fact that the system, under constant loading, has reached a stable state by the re-organisation of the dislocations in the material. Note that the shorter the loading time, the larger the loading duration to get this stable state due to the increase of irreversibilities.

The fourth and last part of this project allowed to reveal the influence of a spatial and temporal discretization, as well as the influence of the loading speed. From this analysis, it was observed that the spatial discretization has no effect whatever the hardening model. Then, by varying the loading speed, it is observed that even for time-independent models, high loading rates induce some numerical errors. It is therefore important to impose a long enough cycle period to avoid those numerical errors. Finally, by varying the time-step, it is once again observed that there is a limit above which errors can occur. Indeed, too large time steps does not allow to capture the different behaviours of the loading.

References

[1] J.Ponthot. *Advanced solid mechanics*, lecture slides MECA0023-1, University of Liège (2021-2022)